



รายงานวิจัยฉบับสมบูรณ์

โครงการ (ภาษาไทย) : การศึกษาแบคทีเรีย Leptospira เชิงบูรณาการ โดยอาศัยวิธีฟิสิกส์เชิงสถิติ การจำลองแบบทางคณิตศาสตร์ การทดลองเชิงคอมพิวเตอร์ และนาโน

เทกโนศาสตร์ : ผลของสนามแม่เหล็กและอนุภาคนาโน

(ภาษาอังกฤษ): The Integrated Studies of Leptospira interrogans using Statistical

Physics, Mathematical Modeling, Computer Simulations and

Nanoscience: effect of magnetic field and nanoparticles

โดย ผศ.คร. วรรณพงษ์ เตรียมโพธิ์

เดือนกรกฎาคม ปี 2550 ที่สำเร็จโครงการ

สัญญาเลขที่ MRG4880161

รายงานวิจัยฉบับสมบูรณ์

โครงการ (ภาษาไทย) : การศึกษาแบคทีเรีย Leptospira เชิงบูรณาการ โดยอาศัยวิธีฟิสิกส์เชิงสถิติ
การจำลองแบบทางคณิตศาสตร์ การทดลองเชิงคอมพิวเตอร์ และนาโน
เทคโนศาสตร์ : ผลของสนามแม่เหล็กและอนุภาคนาโน

(ภาษาอังกฤษ) : The Integrated Studies of Leptospira interrogans using Statistical
Physics, Mathematical Modeling, Computer Simulations and
Nanoscience : effect of magnetic field and nanoparticles

ผู้วิจัย ผศ. ดร. วรรณพงษ์ เตรียมโพธิ์ ภาควิชาฟิสิกส์ คณะวิทยาศาสตร์ มหาวิทยาลัยมหิดล

สนับสนุนโดยสำนักงานกองทุนสนับสนุนการวิจัย

(ความเห็นในรายงานนี้เป็นของผู้วิจัย สกว. ไม่จำเป็นต้องเห็นด้วยเสมอไป)

บทคัดย่อ

รหัสโครงการ: MRG4880161

ชื่อโครงการ: การศึกษาแบททีเรีย Leptospira interrogans เชิงบูรณาการ โดยอาศัยวิธี ฟิสิกส์ เชิงสถิติ การจำลองแบบทางคณิตศาสตร์ การทดลองเชิงคอมพิวเตอร์ และนาโนศาสตร์: ผลของ สนามเหล็กและอนุภาคนาโน

(ชื่อนักวิจัย): นาย วรรณพงษ์ เตรียมโพธิ์

ภาควิชาฟิสิกส์ คณะวิทยาศาสตร์ มหาวิทยาลัยมหิดล

E-mail Address: scwtr@mahidol.ac.th และ wtriampo@yahoo.com

ระยะเวลาโครงการ: 1 สิงหาคม 2548 ถึง 31 กรกฎาคม 2550

Leptospira interrogans เป็นสายพันธุ์หนึ่งในกลุ่ม Leptospira ที่เป็นสาเหตุทำ ให้เกิดโรคเลปโตสไปโรซิส (leptospirosis) หรือโรคฉี่หนู เนื่องจากงานวิจัยส่วนมาก เกี่ยวกับโรคหรือเชื้อโรคชนิดนี้ที่ผ่านมาได้มุ่งเน้นไปที่การรักษาหรือตรวจวินิจฉัยโรคหรือการ ระบสายพันธ์ของเชื้อเป็นสำคัญ ดังนั้นแนวการศึกษาที่ต่างออกไปเพื่อจะนำมาซึ่งความเข้าใจ ต่อโรคและเชื้อโรคชนิดนี้อย่างสมบูรณ์ที่เน้นมิติแห่งการเชื่อมโยงของการศึกษาทางด้าน วิทยาศาสตร์พื้นฐานและและการประยุกต์จึงนับว่าเป็นสิ่งสำคัญมาก ดังนั้นโครงการวิจัยนี้จึงได้ เสนองานวิจัยเชิงบูรณการในเชิงเทคนิควิธีโดยได้ทำการผสมผสานศาสตร์ทางด้านฟิสิกส์เชิง สถิติ การจำลองแบบเชิงคณิตศาสตร์และคอมพิวเตอร์ และศาสตร์นาโนเชิงชีวภาพ เข้าด้วยกัน เพื่อศึกษาแบททีเรียชนิดนี้ กรณีศึกษาจำเพาะได้แก่การศึกษาถึงการตอบสนองของแบททีเรีย Leptospira เมื่อได้รับรังสีอัลตราไวโอเล็ตเอและอนุภาคนาโน ซึ่งปัจจัยทั้งสองอย่างนี้ถือว่า มีบทบาทต่อชีวิตและสิ่งแวดล้อมต่อเราอย่างมาก จากผลการศึกษาทั้งจากากรทดลองและ ทฤษฎีพบว่ามีปรากฏการณ์ใหม่ ๆทั้งที่สามารถอธิบายได้และไม่ได้ที่ยังคงเป็นกรณีศึกษาต่อไป ซึ่งผู้วิจัยเชื่อว่าหากมีการต่อยอดและพัฒนาความรู้ความเข้าใจมากพอจะสามารถ ทำประโยชน์ต่อชุมชนได้อย่างมาก ยิ่งกว่านั้นวิธีวิจัยที่ได้พัฒนาขึ้นนี้ได้ถูกนำไปปรับและ ประยุกต์ใช้กับการศึกษาเกี่ยวกับการเจริญของเซลมะเร็งและการตอบสนองของเซลมะเร็งต่อ ้ตัวกระตุ้นภายนอก ซึ่งถือเป็นการใช้ประโยชน์จากโครงการวิจัยอย่างเต็มที่

คำหลัก: Leptospira interrogans; โรคเลปโตสไปโรซิส; รังสีอัลตราไวโอเล็ต เอ; อนุภาคนาโน; การจำลองแบบ

Abstract

Project Code: MRG4880161

Project Title: The Integrated Studies of Leptospira interrogans using Statistical Physics,

Mathematical Modeling, Computer Simulations and Nanoscience: effect of magnetic

field and nanoparticles

Investigator: Mr. Wannapong Triampo

Department of Physics, Faculty of Science, Mahidol University

E-mail Address: scwtr@mahidol.ac.th and wtriampo@yahoo.com

Project Period: 1 August, 2005-31 July, 2007 (2 years)

Leptospira interrogans are pathogenic leptospires that cause leptospirosis, a worldwide zoonotic disease. Since most researches on this disease have been focused on the clinical and diagnostic aspects, to fulfill the spectrum of understanding this disease and to try bridges the gap between medical or clinical facts and basic sciences is of crucially important. Therefore, we propose to use the integrated approach consisting statistical physics, mathematical modeling, computer simulations and biological nano-science as new means to primarily study these bacteria. With these tools, the specific problems namely, the studies of the effects of ultraviolet A and TiO2 nano-particles on Leptospira were performed. These effects currently have such great impacts on our life and environment. Our findings revealed several new information regarding to these bacteria interacting with the imposed stresses. However, the results lead to several unanswered interesting questions and yet to be investigated. We believe that the new findings from these works could be developed and optimized to benefit the community. Moreover, most developed protocols were also applied to study the response of cancer cells to the interested stress to maximize the benefits from the project.

Keywords: Leptospira interrogans; leptospirosis; ultraviolet A; nanoparticles; modeling

1. EXECUTIVE SUMMARY

In this project we propose to use the integrated approach consisting statistical physics, mathematical modeling, computer simulations and biological nano-science as new means to primarily study these bacteria. With these tools, the specific problems namely, the studies of the effects of ultraviolet A and TiO₂ nano-particles on *Leptospira* were performed. These effects currently have such great impacts on our life and environment. Moreover, the developed protocols were applied to study the response of cancer cells to the interested stress to maximize the benefits from the project. To summarize our project consists of 3 sub-projects according to problem-based: 1) the effects of UV on *Leptospira* 2) the effects of TiO₂ nanoparticles on *Leptospira* 3) the effects of TiO₂ nanoparticles on cancer cells. Our findings revealed several new information regarding to these bacteria interacting with the imposed stresses. However, the results lead to several unanswered interesting questions and yet to be investigated.

The outputs from this project are quite satisfactory. There are 15 pieces of works all together with five of them are either published or accepted articles. With experiences gained from this research project, it provides and builds us enough knowledge and potential to write a very fine book for the students.

Lastly, we would like to mention that we believe that because of the integrated and multidisciplinary kind of this (unique) research project, it then open up the door of opportunity to the researchers to explore and utilize all possible his or her skills to attack to problems. At least with this work, it made us know how much we need to improve ourselves and in what way.

2. BACKGROUND AND RATIONALE (for main project)

Leptospirosis is an acute febrile illness caused by pathogenic spirochetal bacteria of genus *Leptospira* and species *Leptospira interrogans* [Faine (1982), Faine (1999)](see appendix for more details). This disease has emerged as an important public health problem worldwide. The illness resulting from this disease can range from being a mild flu-like illness to being a severe (often fatal) disease involving renal and/or liver failures and hemorrhages (referred to as Weil's syndrome) [Sherris (1984)]. Most outbreaks tend to be seasonal in nature and are often linked to environment factors, to animals and to agricultural and occupational cycles like cultivating rice in marshy land. Mammals such as rats and cattle are commonly involved in the transmission of this disease to human via direct or indirect exposure to contaminated tissues or urine[Faine (1982), Faine (1999), Turner (1967)]. Out-breaks of leptospirosis occur mainly after flooding, leading it to becoming an occupational hazard for sanitary and agricultural workers as well as a recreational hazard for humans.

Thailand is one of the agricultural and tropical countries which is prone to this disease. In the last ten years there has been an outbreak of this disease at least every other year. There has been a trend for the infection to become greater each year. Since there are so many pathogenic serovars, it is so difficult to make vaccine. Thus so far, there is no vaccine for human to protect us from this disease. For this, the best strategy to control the disease is still being sough.

Most researches on this disease have been focused on the clinical and diagnostic aspects. To fill the spectrum of understanding this disease and to try bridge the gap between known facts and still opened-question, We wish to apply "unconventional" tools to the study of this disease. We propose to use Integrated approach consisting statistical physics, mathematical modeling, computer simulations and Medical nanoscience as new means to study this problem.

We will focus on the Leptospira bacteria, *Leptospira interrogans especially* serovar *canicola* in this study. The proposed approach will be used to investigate the nature of *L. interrogans* in four cases. There are (1) cell morphology at micro and nano-scale (2) cell motility mechanism and (3) the interaction between the leptospires and its surrounding i.e., how bacteria response to the "perturbed" physical and chemical nanoparticle tudies will closely link to microbiological, epidemiologic, clinical, and pathological approach. All four topics will be analyzed in terms of both the dynamic(time dependent) and static(time independent) behaviors, uses both deterministic and stochastic techniques, as well as both from "wet" lab and "dry" lab hand-on.

3. PROJECT OBJECTIVES

With the integrated tools, the specific objectives of this proposed research work are as follows.

- 1. To have more insight into the morphology and surface physical properties at micro and nanoscale resolution in conjunction with the related cell physiology
- 2. To gain more understanding about mechanism of cell motility of leptospire and be able to purpose reasonable model (at least base line model) for this properties.
- 3. To stochastically model for understanding the experimental results from 1 to 3 using mainly statistical physics
- 4. To do comparison studies of 1-4 using the different environmental conditions e.g., magnetic field and nanopartoicles
- 5. To develop the integrated tools of life science research

4. RESEARCH ACTIVITIES

• Subproject 1: Effects of UVA on Leptospira

Summary: The effect of exposure of ultaviolet-A (UVA) radiation was studied on the pathogenic spirochetes Leptospira interrogans serovar Canicola for different time durations. The changes in cell growth and viability due to the UVA exposure were determined by using conventional microscopic agglutination test (MAT), dark-field microscopy and spectrophotometry measurements. Changes in antigens and protein expression in the cells were detected by sodium dodecylsulfate polyacrylamide gel electrophoresis (SDS-PAGE) and immunoblot. The decrease in cell growth and viability were found to be exposure period or dose dependent. The growth decreased sharply with very high rate for the first 24 h of exposure, then the growth reached the minimum within about 1d exposure period and level-off for the further treatment until 7d exposure period. Immunoblot revealed the presence of 21 kDa antigenic protein in the unexposed cells, which disappeared after exposure to UVA of 24 h. SDS-PAGE analysis indicated the presence of the 76 kDa protein band in the cells exposed to UVA for 2 h to 24h. For more than 2h to 24h exposure to UVA decreased this protein, but the proteins of molecular mass between 56 kDa and 70 kDa appeared. This work is the first step toward the understanding of the effects of UVA on leptospira bacteria. With further investigations especially about mechanisms of how UVA interact with leptospira, it will eventually lead to development of new strategies to control or prevent leptospira in the environment.

Materials and Methods

Strain and culture conditions of leptospira

Pathogenic *Leptospira interrogans* serovar Canicola were obtained from the National Leptospirosis Reference Center, National Institute of Health (NIH), Thailand and grown in the Ellinghausen and McCullough liquid medium as modified by Johnson and Harris (EMJH)^{8,19} at about 27°C. The samples were sub-cultured on a weekly interval. Each of 3 ml bacterial culture in 1.5 cm diameter glass tube had an initial optical density (OD) at 400 nm of about 0.10, as measured by a UV-VIS spectrophotometer. This was equivalent to 1+ level as graded using a dark-field microscope which in turn indicated a cell concentration of ~10⁸ cells/ml.

UVA irradiation source

The UVA radiation was generated by a 20 W T12 fluorescent lamp, Backlight (Sylvania Co.). The lamp produced a continuous emission spectrum (320-400 nm) and a peak at 365 nm, measured by HR2000CG-UV-NIR high-resolution composite-grating Spectrometer (Ocean Optics, Inc.). The UVB and UVC radiations were absorbed by the glass tube. The experimental leptospira samples were exposed to UVA radiation of intensity of about 1.3 mW/cm², as measured by a 1830-C optical power meter with detector and calibration module model 818-UV/CM (Newport Corporation.).

Irradiation procedure

Separate leptospira samples were exposed to UVA at a distance 20 cm from the source of radiation for 0, 5, 15, 30, 45, 60, 120, 180 and 360 min on day 1, and for several more days (1 to 7 days). After exposure, all cultured samples were maintained for a further 7 days. On 7th day post-treatment, all the samples were taken for measurements of their viability and growth using a dark-field microscope (Axiloab Pol 2, Carl Zeizz Co.) mounted with a CCD camera. Micrographs were taken using the AxioVision AC 4.1 software. Semi-quantitative techniques based on microscopic agglutination test (MAT), turbidity-based method, UV-VIS spectrometer were also employed. Protein or antigenic changes were determined by using SDS-PAGE. Experiments were repeated at three times under the same conditions with separated occasions.

Growth and cell survival

The techniques mentioned above were used to monitor the bacterial growth and survival.

Qualitative analysis by dark-field microscopy

The growth and survival of treated leptospira were determined by looking at cell density, mobility ²⁰ and morphology. Since due to their very thin size and poor uptake of conventional dyes, leptospira could not be observed by ordinary light microscope, dark-field microscopy (DFM) was used ⁴. In DFM, an oblique light beam was cast on to the leptospira (lying on a microscope slide) using a special condenser, when the central illuminating light beam was interrupted. The leptospira could then be seen as silvery threads in a dark background. To assess the effect of UVA on the

growth and survival, samples were diluted 10-fold on 7th day post-treatment and were observed with a dark-field microscope.

Semi-quantitative analysis by microscopic agglutination test (MAT)

MAT is a standard serological technique used in the diagnosis of leptospirosis⁴. It is used in combination with the enzyme-linked immunosorbent assay (ELISA). It is a reference test and is used to detect the presence of the antibodies and determine their titer. It can also be used to determine relative growth of bacteria colony. The method is simple and consists of mixing the test serum with a culture of leptospira and then evaluating degree of agglutination using a dark-field microscope.

The reference-specific antiserum against L. interogans serovar Canicola was required for the test. Leptospira samples were mixed with 2-fold dilutions of antiserum (1:100, 1:200, 1:400, 1:800, 1:1600, 1:3200, 1:6400) and incubated for 2 h at room temperature. The agglutination reactions were then observed under a 200x dark-field microscope and scored as follows: 4+, 3+, 2+, 1+ = 100%, 75%, 50%, 25% absence of free leptospira from the field, respectively.

Quantitative analysis by UV-VIS spectroscopy

An UV-VIS spectrometer (V-530 UV/VIS spectrometer, Jasco InternationI Co., Ltd.) was used to quantify the amount of *Leptospira* present by light absorption measurement in the UV-VIS spectrum ^{8,21,22}. These were done on exposed leptospira cells (for different exposure times) taken on the 7th day of their cultivation. Solutions of the leptospira cells were placed into cuvettes made with quartz SUPRASIL (200-2500 nm) with light path 10 mm (type no. 100.600-QG, Hellma Co.). A single beam spectrometer operating in the range of 200-800 nm was used. The OD or absorbency at 400 nm was taken ²¹. All samples were obtained with already used EMJH liquid medium as the blank.

Scanning electron microscopy (SEM)

Samples were washed three times with normal saline (0.9% NaCl) at $10,000 \times g$ for 10 min and dropped on poly-L-lysine-coated cover glass slide for 1 h. Samples were prefixed directly with 2.5% glutaraldehyde for 2 h at room temperature and then washed three times with 0.01 M phosphate buffer (pH 7.3) for 10 min. All samples were post-fixed with 0.1% osmium tetroxide. After fixation, samples were dehydrated with increasing concentrations of ethanol, critical point-dried (HPC-2 critical point dryer, Hitachi), and coated with platinum-palladium ion sputter (E102 ion sputter, Hitachi) for 2 min. The micrographs were taken with accelerating voltage of 15 kV SEM (S2500, Hitachi) on the negative film.

SDS-PAGE and immunoblot

Leptospiral cultures were centrifuged at 10, $000 \times g$ for 10 min and the pellets were washed three times in normal saline (0.9% NaCl) and then solublized in SDS-PAGE sample buffer

composed of 0.35 M Tris.Cl (pH 6.8), 10% SDS, 30% glycerol, 9.3% dithiothreitol (DTT) and 0.175 mM bromophenol blue 23 .

For one-dimensional SDS-PAGE, other samples were solubilized in SDS-PAGE sample buffer. The samples were heated at 100°C for 10 min²³. The 3 µl of each sample was loaded on to 12% polyacrylamide gels²⁴ and electrophoresed at 200 voltages for 55 min. The molecular mass protein standards (Amersham) used were: rabbit muscle phosphorylase B (97 kDa), bovine serum albumin (66 kDa), hen egg-white ovalbumin (45 kDa), bovine carbonic anhydrase (31 kDa), soybean trypsin inhibitor (20 kDa), and hen egg-white lysozyme (14 kDa). After electrophoresis, gel was separated into two parts. One part was stained with Coomasie brilliant blue (0.025% Coomassie R-250, 40% methanol, 7% acetic acid) for 1 h and then destained with destaining solution I (40% methanol, 7% acetic acid) for 1 h and fixed with destaining solution II (5% methanol, 7% acetic acid). The other part was blotted on to a polyvinylidene difluoride (PVDF) membrane at 1.6 mA/cm² for 70 min. After transfer, membranes was incubated with 0.1%(w/v) Ponceau S in 5% (v/v) acetic acid (Merck) and washed with 2% skimmed milk and 0.2% tween20 (Sigma, USA) in phosphate buffer saline (PBS).

For immunological detection, the membrane was incubated with primary antibody (rabbit reference antiserum specific to L. interrogans serovar Canicola) at 1:1,000 dilutions in 2% skimmed milk and 0.2% tween20 in PBS for 1 h, and washed three times for 10 min each in 2% skim milk and 0.2 % tween20 in PBS. Thereafter, the membrane was transferred to a solution of secondary antibody [polyclonal goat anti rabbit immunoglobulin HPR (DakoCytomation P0448)] at 1: 2,000 in 2% skimmed milk and 0.2% tween20 in PBS, incubated for 1 h, and then washed three times for 5 min each in PBS. Color was developed with a solution of 1.25 mg of diaminobenzidine (DAB) and 5 μ I of 35% H_2O_2 in 10 ml of PBS. The membrane was then rinsed in several changes of PBS to stop the reaction, air-dried and photographed.

Subproject 2: Antibacterial effects of TiO nanoparticles combine with UVA on Letospira interrogans

Summary: TiO_2 nanoparticles (TiO_2 -NP) combine with Ultraviolet-A (UVA) radiation were recently reported as the photocatalytic disinfection process. Our study is to investigate the antimicrobial effects of TiO_2 -NP on *L. interrogans* serovar Canicola represented as pathogenic leptospires that cause leptospirosis. The bacteria were cultured and treated by TiO_2 -NP, UVA radiation at variable time duration of 2, 6 and 24 hr with and without TiO_2 -NP at 50 μ g/~108cells-ml. The results show that samples with higher dose UVA (112.3 W-sec/cm2) both with and without TiO_2 -NP have higher antimicrobial effects resulting in the decrease in the growth and viability of bacteria when compared with those without UVA exposure. By immunoblotting method, Leptospiral antigen components about

21 and 48 kDa disappear when compared with non-exposed control. Only TiO₂ treatment alone does not significantly give any difference from the control (no treatment) samples. From our preliminary works, it may be concluded that the UVA play a major role on antimicrobial effects while the TiO₂-NP affect bacteria only when photocatalysis is occurred. Further studies with TiO₂-NP must be carried out using such as different doses and/or exposure periods if we want to reach a better understanding.

Materials and Methods

Experiments

We shall perform the "wet" lab experiments repeatedly starting with cell culturing which are grown in an EMJH liquid medium using the method of Ellinghausen and McCullough, as modified by Johnson and Harris at a temperature of 27±1°C in the dark. With the appropriate and optimal specimen preparation, we will

- Perform an extensive nano-scale morphological and membrane studies using AFM and other microscopy under controlled and varied (e.g.magnetic, nanoparticles) conditions.
- ii. Perform the studies of cell division using "magnetic field frozen technique", dark-field microscope, agglutination reaction technique (MAT) technique, and nano-scale studies using AFM
- iii. Perform the cell motility studies under various condition using the cell cultured and compound microscope with high performance CCD camera for image capturing and appropriate software for image processing and data analysis.
- iv. Perform the anti-leptospire material properties experiment using TiO₂ as a primary agent and MAT test as primary test together with the turbidity quantification.

Data analysis

- Use analysis of variance technique through the SPSS package as primary statistical tools
- ii. Apply fractal analysis to characterize the morphology and roughness of cell and use ImageJ (free US. nih) software as a primary fractal analysis tools.
- iii. Perform data Regression tools via appropriate numerical analysis technique.
- iv. Conduct scaling analysis for non-equilibrium nature studies

Stochastic Models

- i. Perform the stochastic mathematical and computer modeling of cell division mechanism under various condition
- ii. Perform the stochastic mathematical and computer modeling of cell motility under various conditions.
- iii. Perform the stochastic mathematical and computer modeling of antileptospira material properties using TiO₂ nanoparticles as a main material.

Subproject 3: Effect of TiO₂ Nanoparticleson on cancer cells

Summary: With the breakthrough of nanotechnology and increasing use of nanoparticles(NPs)in commerce, there are however few investigation about the cytotoxicity of NPs for health and risk concerns. Specifically, semiconductor nanopaticles like TiO₂ nanoparticles(TiO₂-NPs) have become a new generation of advanced materials due to their novel and interesting optical, dielectric, and photocatalytic properties resulting in many well known applications such as cosmetics, foods and painting colors etc..

In this work, the cytotoxic effects of TiO_2 -NPs on the survival and growth of human cervical carcinoma(HeLa) cells are studied. The dose-dependent effect is monitored by varying does from 25 to 400 µg/ml. Various qualitative and quantitative characterization techniques including colony-forming assay and image processing technique are used to tackle this problem both from biological and biophysical aspects. The results show that even in the dark condition(no photocatalytic reaction), for TiO_2 -NPs treated condition at high enough concentration(>150µg/ml), a number of surviving colonies are significantly decreased. Morphologically, the colony size reduction and colony shape deformation are also reported (ANOVA, p<0.001). This seems to indicate that TiO_2 -NPs can interfere normal activity of HeLa cells *in vitro*. i.e., proliferative activity may be disrupted that leads to abnormal growth.

Materials and methods

Cell culture

Human cervical carcinoma cells(HeLa), obtained from National Cancer Institute, Thailand, were cultured in EMEM(BioWhittaker), pH 7.2, supplemented with 10% NCS(BioWhittaker), penicillin(100 U/ml) and streptomycin(100 µg/ml) at 37°C in a humidified atmosphere of 5% CO₂.

Chemical

TiO₂-NPs(P25, Sigma-Aldrich) with a surface area of 10-20 m²/g and primary particles whose size of 60-100 nm were used in experiments. The particles were suspended in sterile water and sonicated for 15 min before experiment. All processes were performed in darkness.

Colony-forming assay and treatment

HeLa cells in exponential phase were trysinised and counted by Hemocytometer. Then cell suspension was diluted and plated in 6 well culture cluster(Corning) with a density of 100 cell/well. The various concentration of TiO_2 -NPs(25-400 μ g/ml) was added and sterile water was used as control. Cells were incubated at 37°C in a humidified atmosphere of 5% CO_2 .

Measurement of serving fraction and morphological changes

After culture for 10 days, The colonies were stained with 10% Giemsa solution(Merk) and counted. Plating efficiency(PE) and surviving fraction were calculated by formulas as follow.

Plating efficiency =
$$\frac{Number\ of\ colonies\ counted}{Number\ of\ cells\ seeded} \times 100\%$$

Surviving fraction =
$$\frac{Number\ of\ colonies\ counted}{Number\ of\ control-colonies}$$

Then colonies were photographed under stereo microscope(Stemi 2000-C, Zeiss) at 12.5x magnification and the images were analyzed by Image-Pro[®]3DS version 5.1.2.59.

3. Results

Serving fraction

After cells were treated with TiO_2 -NPs, surviving was reduced with dose-dependent, plating efficiency = 83%. The survival rate will less than 50% when it is treated with TiO_2 -NPs that has concentration greater than 150 μ g/ml (*figure 1*)

Colonies size

The result shows the change in colonies size distribution(figure 2a, Left). When TiO₂-NPs concentration in culture is increased, a colonies diameter distribution is shift to left hand side which means colonies size is reduced. To emphasize the colony size reduction we have shown the picture

of colonies that have a diameter equally to an average in each group($figure\ 2a,\ Right$). The statistical test shows TiO_2 -NPs can reduce a diameter of colonies significantly(ANOVA, p<0.001 and follow by LSD, p<0.05) and the reduction curve can fit with exponential decay function, $figure\ 2b$. It indicates that a diameter of colonies will decrease rapidly when TiO_2 -NPs concentration increases.

In *figure 3*, colonies were divided into 3 classes according to their size which are small colony(Colony diameter < 400 μ m), medium colony(Colony diameter is 400-600 μ m) and large colony(Colony diameter > 600 μ m). When TiO₂-NPs concentration is increase, the proportion of small colonies will rise from 21.3% in control to 100% in the highest treated-dose, 400 μ g/ml. In contrast, the proportion of large colonies will reduce from 21.3% in control and disappear when TiO₂-NPs concentration is higher than 150 μ g/ml. According to the proportional change of these three colony classes indicate that cancer colonies can not grow from small to be a medium colonies or from medium to be a large colonies in the present of TiO₂-NPs.

Axis ratio

Axis ratio, the proportion between minor axis and major axis, was used to infer circularity of colony. This value will equal 1 when colony shape is circle. If colony is deformed, the value will reduce. As present in *figure 4*, axis ratio was reduced significantly (ANOVA, p<0.001 and follow by LSD, p<0.05) when cells were exposed to TiO_2 -NPs. Moreover, the reduction can be fitted with Gaussian function.

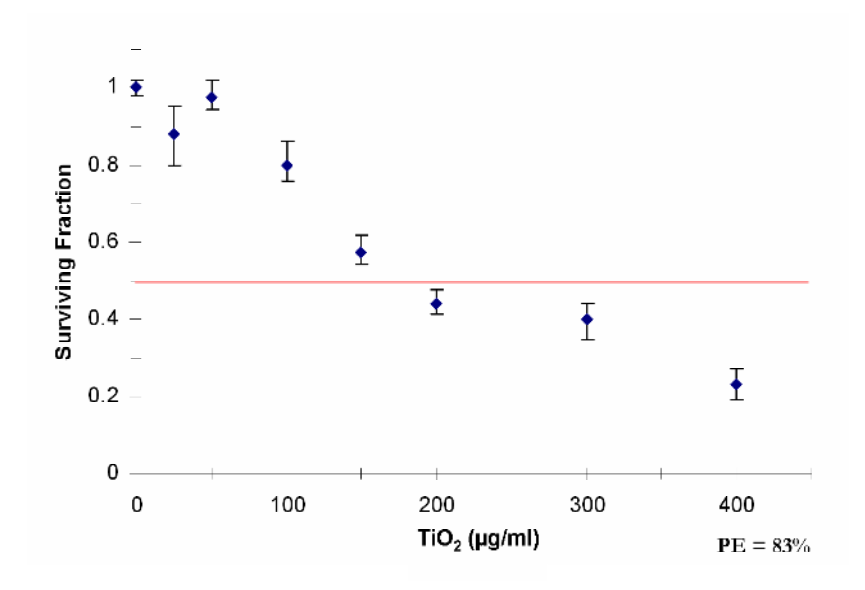


Figure 1 Survival curve of Hela cells after were treated by TiO_2 -NPs, plating efficiency = 83%. Surviving fraction was reduced and survival rate will less than 50% when concentration of TiO_2 -NPs > 150 μ g/ml

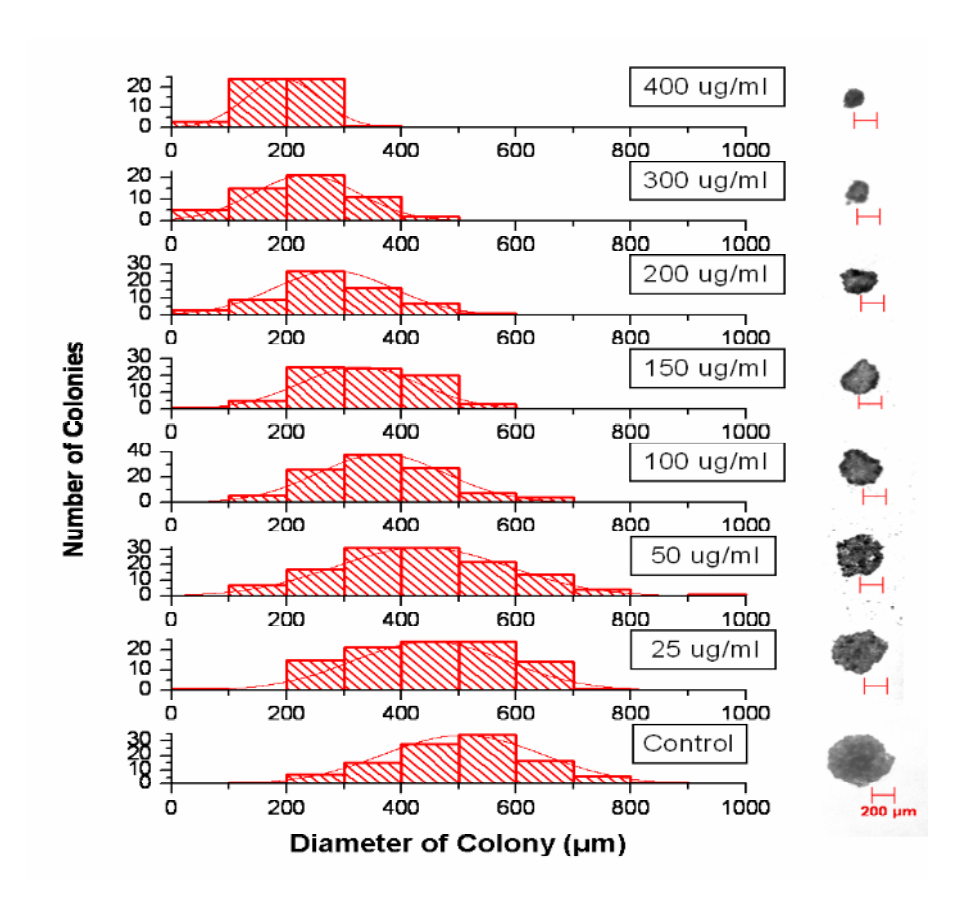


Figure 2a Histogram shows the effects of TiO₂-NPs on the size of cancer colonies(*Left*). When TiO₂-NPs concentration is increased, the distribution was shift to left hand side which shows the size reduction. The picture of colonies that have a diameter equally to an average in each group is shown in *right*.

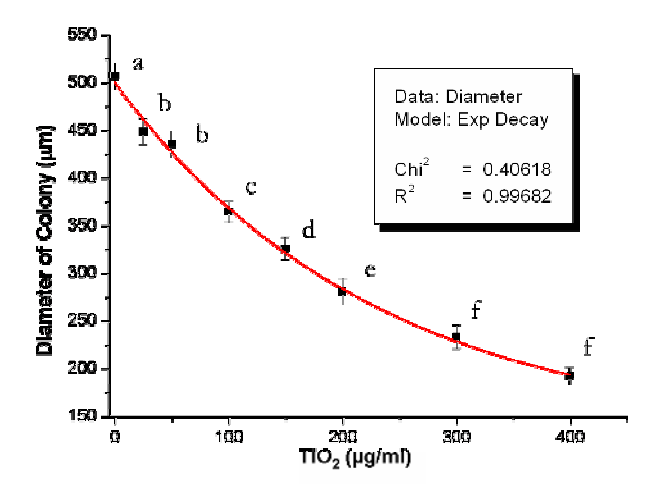


Figure 2b $\text{TiO}_2\text{-NPs}$ can reduce a diameter of colonies significantly(ANOVA, p<0.001 and follow by LSD, p<0.05) and the reduction curve can fit with exponential decay function. It indicates that a diameter of colonies will decrease rapidly when $\text{TiO}_2\text{-NPs}$ concentration increases.

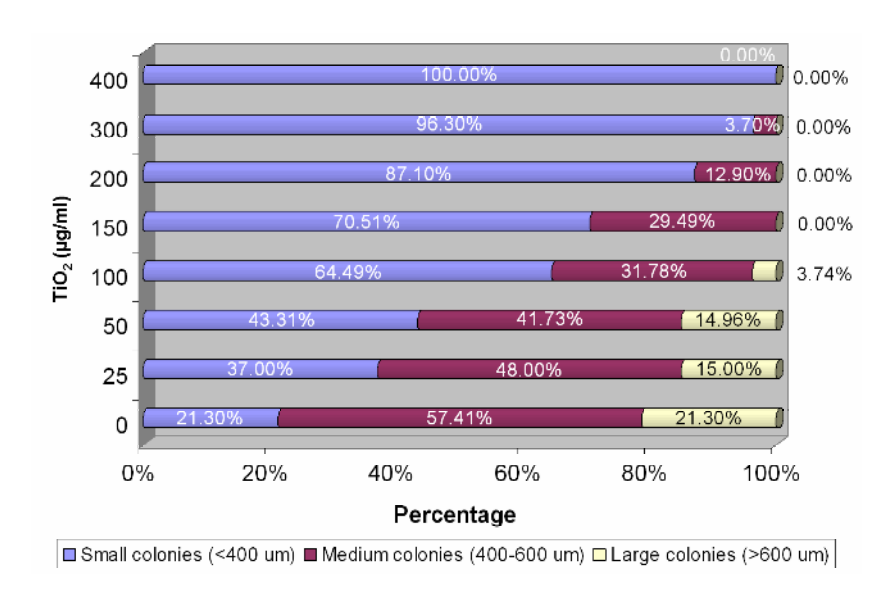


Figure 3 Colonies were divided into 3 classes according to their size which are small colony(Colony diameter < 400 μm), medium colony(Colony diameter is 400-600 μm) and large colony(Colony diameter > 600 μm). The result shows a proportional change of these three colony classes. When TiO_2 -NPs concentration is increase, the proportion of small colonies will rise from 21.3% in control to 100% in the highest treated-dose, 400 μg/ml. In contrast, the proportion of large colonies will reduce from 21.3% in control and disappear when TiO_2 -NPs concentration is higher than 150 μg/ml.

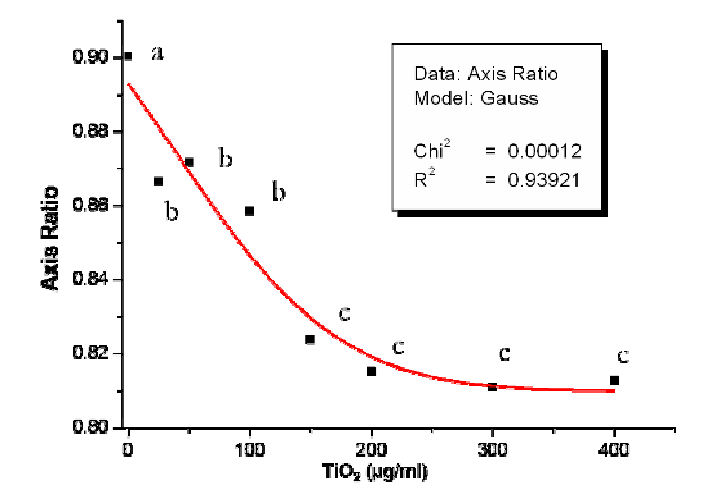


Figure 4 After cells were exposed to TiO_2 -NPs, axis ratio was decreased significantly(ANOVA, p<0.001 and follow by LSD, p<0.05) and a curve can be fitted with Gaussian function.

Note: More details and outputs see the attached documents.

5. Output

ประเภทของ	ระบุรายชื่อและการอ้างอิง	
output		
ผลงานในวารสารสาร	PUBLISHED OR ACCEPTED Papers	
นานาชาติ	P1: Boondirek A.,Wong-ekkabut J., Triampo W., Tang	
	IM., Picha P, and Lenbury Y. A Stochastic Model of	
	Cancer Growth with Immune Response, J. Korean Phys.	
	Soc. 2006; 45(2): 310-317	
	P2: Triampo,W., Baowan, D., Tang ,I.M., Nuttavut,N.,	
	Wong-Ekkabut, J., Doungchawee,G., A Simple	
	Deterministic Model for the Spread of Leptospirosis in	
	Thailand. International Journal of Biomedical Sciences,	
	2007, 2(1):1306-1216	
	P3: Sungkaworn,T., Triampo,W., Nalakarn,P.,Triampo,	
	D., Tang ,I. M., Lenbury, Y., and Picha, P., Effect of TiO2	
	Nanoparticle Aggregates on Tumor Cell Colonies: Fractal	
	Dimension and Morphological Properties. International	
	Journal of Biomedical Sciences, 2007, 2(1):1306-1216	
	P4: Triampo, D., Triampo, W., Tang, I.M., and Lenbury,	
	Y., The Stochastic Model of Non-equilibrium Mutagen-	
	induced Alterations of DNA: Implication to Genetic	
	Instability in Cancer. BioSystems (2007)	
	P5: Wong-ekkabut, J., Xu, Z., Triampo, W., Tang, I.M.,	
	Tieleman, P., and Monticelli, L., Effect of Lipid	
	Peroxidation on the Properties of Lipid Bilayers: a	
	Molecular Dynamics Study, accepted Biophysical Journal.	
	(2007)	

IN REVISION papers

R1: Modchang, C., Triampo,W., Kangthang, P., Junthorn, U., Unai, S., Ngamsaad, W., Nuttawut, N., Lenbury,Y., Stochastic Modeling of the Effect of an External Electric Field on the Min Protein Dynamics in E. coli, submitted to Biosystems. (2007)

R2: Wong-ekkabut, J., Triampo, W., Baowan, D., Chadsuthia, S., Doungchawee, G.,Krittanai, C., and Tang, I.M., Response of Pathogenic Spirochete Leptospira Interrogans Serovar Canicola to Ultaviolet-A Irradiation, Indian Journal of Biochemistry and Biophysics (IJBB), in revision (2007)

SUBMITTED papers

S1: Unai, S., Kanthang, P., Junthona, U., Ngamsaad, W., Triampo, W., Modchang, C., Kritanai, C., and Lenbury, Y., The Dynamics and Localization of MinD Protein Oscillations Through the Single Particle Tracking, submitted to Biophysical Journal . (2007)

ผลงานนำเสนอประชุม วิชาการ

C1: Apiwat Wisitsorasak 1, Wannapong Triampo,
Monte Carlo simulations of signal transduction mediated
by G-protein:spatial distribution of molecules,
32nd Congress on Science and Technology of Thailand
(STT.32) 10 - 12 October 2006, at Queen Sirikit National
Convention Center, Bangkok, Thailand

C2: Harit Pitakjakpipop, Wannapong Triampo, Lakana Himakoun, Environmental effects of nanoparticles: geotoxic effects of titatnium dioxide on induction of micronucleus formation in the snake head fish cell line, 32nd Congress on Science and Technology of Thailand (STT.32) 10 - 12 October 2006, at Queen Sirikit National Convention Center, Bangkok, Thailand

C3: Sudarat Chadsuthi, Wannapong Triampo, Galayanee			
Doungchawee, Jirasak Wong-ekkabut, Antibacterial			
effects of TiO ₂ nanoparticles combine with UVA on Letospira interrogans serovar Canicola, 32 nd Congress on Science and Technology of Thailand			
		(STT.32) 10 - 12 October 2006, at Queen Sirikit National	
		Convention Center, Bangkok, Thailand	
C4: Jirasak Wong-Ekkabut,L Monticelli,Z. Xu,			
S.Baoukina,W. Triampo, I.M. Tang, P. Tieleman, Effect of			
perocidation on the properties of a palmitoyl-2-linoleyl-sn-			
glycero-3-plosphatidylcholine bilayer . 51th Annual			
Meeting Biophysical Society , Baltimore, Maryland ,March			
3-7, 2007			
C5: S Unai P Khantang U Junthorn W Ngamsaad N			
THAILAND			
C6: S. Chadsuthi, W. Triampo, G. Doungchawee, J. Wong-			
ekkabut, D.Triampo, and I. M. Tang, Effect of TiO2			
Nanoparticles on Pathogenic Spirochetes, Leptospira			
Interrogans. SIAM PHYSICS CONGRESS 2007, March 22			
–24, Nakorn Pathom, THAILAND			
วรรณพงษ์ เตรียมโพธิ์ , นาโนเทคโนโลยี, สารานุกรมไทย			
้ สำหรับเยาวชน โดยพระราชประสงค์ในพระบาทสมเด็จพระ			
เจ้าอยู่หัว เล่มที่ ๓๒ เดือนสิงหาคม ๒๕๕0			
	Doungchawee, Jirasak Wong-ekkabut, Antibacterial effects of TiO ₂ nanoparticles combine with UVA on Letospira interrogans serovar Canicola, 32 nd Congress on Science and Technology of Thailand (STT.32) 10 - 12 October 2006, at Queen Sirikit National Convention Center, Bangkok, Thailand C4: Jirasak Wong-Ekkabut, L Monticelli, Z. Xu, S.Baoukina, W. Triampo, I.M. Tang, P. Tieleman, Effect of perocidation on the properties of a palmitoyl-2-linoleyl-sn-glycero-3-plosphatidylcholine bilayer . 51th Annual Meeting Biophysical Society , Baltimore, Maryland ,March 3-7, 2007 C5: S.Unai, P. Khantang, U. Junthorn, W. Ngamsaad, N. Nattavut, W. Triampo, and C. Krittanai, Biophysical Study of MinD Protein Oscillation in E. coli. SIAM PHYSICS CONGRESS 2007, March 22 –24, Nakorn Pathom, THAILAND C6: S. Chadsuthi, W. Triampo, G. Doungchawee, J. Wongekkabut, D.Triampo, and I. M. Tang, Effect of TiO2 Nanoparticles on Pathogenic Spirochetes, Leptospira Interrogans. SIAM PHYSICS CONGRESS 2007, March 22 –24, Nakorn Pathom, THAILAND		

6. APPENDICES

The following attachments are the output as mentioned in the previous sections.

A Stochastic Model of Cancer Growth with Immune Response

A. Boondirek and Y. Lenbury

Department of Mathematics, Faculty of Science, Mahidol University, Bangkok 10400, Thailand

J. Wong-ekkabut

Department of Physics, Faculty of Science, Mahidol University, Bangkok 10400, Thailand

W. Triampo*

Capability Building Unit in Nanoscience and Nanotechnology, Faculty of Science, Mahidol University, Bangkok, 10400, Thailand

I. M. Tang

Institute of Science and Technology for Research and Development, Mahidol University, Nakhonpathom 73170, Thailand

P. Picha

National Cancer Institute of Thailand, Bangkok 10400, Thailand

(Received 1 April 2006, in final form 12 July 2006)

A cellular automaton model for the growth of an avascular tumor on a two-dimensional square lattice is presented. The pattern formation and the growth of the cell population are investigated by using a Monte Carlo simulation. A microscopic description of the immune system response, including cell proliferation, cell death, and cell degradation, is used to simulate the growth. In particular, the escape rate for cancer from immune surveillance is included for consistency with experimental observations. The simulation results give rise to a growth curve with an explanation on a microscopic scale that is shown to agree well with experimental animal tumor growth and relevant biological implications. Our model clearly shows that an increase in the lysis rate leads to a decrease in the proliferation rate of cancer cells. The spatial distribution of proliferated cell and the fractal dimension of the boundary are also measured.

PACS numbers: 87.15.Aa, 87.17.Aa

Keywords: Cancer growth, Immune response, Cellular automaton, Monte Carlo, Gompertz curve

I. INTRODUCTION

Cancer has been a leading cause of human death in the world. There is not too much known about the biological mechanisms leading to the establishment of or the growth of malignant tumors. Many attempts have been made in recent decades to describe the basic biological mechanisms of tumor growth.

Most tumor growth models were proposed to investigate one or several basic features, such as the cell cycle, the cell proliferation, the lack of nutrients, the competition for resources, and the cytotoxic activity by the immune response [1–29]. Two types of approaches have been used to describe the growth of the tumor: the continuous models [17,30] and discrete models [1–4,8,15,22,27–29,31]. A few discrete models have used

an automaton-based method. These cellular automaton (CA) models are based on the properties of the actual cells at the cellular level, that is, the microscopic scale. The CA models use microscopic-scale information to determine the cellular automata rules by applying the rules for each time step in an iterative manner. In this way, the CA models, which use the Monte Carlo approach to the cell dynamics, might be called Monte Carlo Cellular Automaton models. This approach is also well known to be very useful for a myriad of stochastic process applications [32,33].

One of the cancer growth modelling aspects is the immune response. However, the precise natural complexity of the immune response remains poorly understood. Many studies have established that the immune response plays a crucial role in eliminating cancer cells from healthy tissues [23,26,34–37]. A number of authors [23,26], Bell [35–37] have focused on the details at the cellular level of immune cell binding and delivery of lethal

^{*}E-mail: scwtr@mahidol.ac.th; Fax: +66-2-201-5843

hits. In particular, in 1984 Lefever and Erneaux [23] proposed a reaction diffusion formulation of the growth of cancerous tissue attacked by immune cytotoxic cells they used a system of kinetic equations for cell growth and cell-mediated cytolysis in tumors composed of a two-step reaction for the kinetics of cell-mediated cytolysis in tumors. This reaction led only to the tumor-immune cell complexes producing either dead tumor cells or immune cells

In 1994, Kuznetsov and Taylor [21] proposed a new model for the tumor-immune interaction, which included the two step reactions in Ref [23]. What was new in Kuznetsov and Taylor's model (KT model) was the detachment (or breaking up) of tumor-immune cell complexes from each other. The detachment of the complexes was assumed to occur without damaging the tumor cell, inactivating the immune cell, changing the programming for the lysis of tumor cell, or activating an immune cell to become cancerous. Several assumptions made by Kuznetsonov and Taylor [21] have lead several researchers, like Matzavinos and Chaplain [10,11] Galach [14] to develop new models to investigate the dynamics of tumor-immune system competition.

Qi et al. [1] developed a cellular automaton model of cancerous growth with a microscopic description applying a system of kinetic equations for the growth and cellmediated cytolysis in tumors proposed by Lefever and Erneaux [23] including the mechanical pressure arising from within the tumor [38]. They attempted to provide a microscopic explanation for the Gompertz growth by establishing a set of probabilistic cellular automaton (PCA) rules. Their simulated results produced a Gompertzian growth curve with a significant fluctuating component.

The major purpose of this research is to further develop the CA model of Qi et al. [1] to include more realistic biological implications from the KT model. In particular, we create a novel fundamental kinetics model of tumor growth while neglecting the behavior of the mechanical pressure. The new fundamental kinetics model is able to describe the interaction and the competition between the tumor and the immune system. Additionally, our model takes into account tumor-cell proliferation, the tumor's interaction with the immune system, resulting in either lysis of the proliferating tumor cells or the detachment of immune binding without damaging the cancer cells, as well as the removal of dead tumor cells in avascular tumors. By adding the detachment of immune binding without damaging cancer cells, we found a different result from Qi et al. [1] with regard to the variation of the lysis rate. A large lysis rate gives a lower number of proliferating cancer cells. This agree well, in particular, with the experimental results from hormonal therapy with tamoxifen [39,40]. We have neglected the presence of inactivated tumor-infiltrating cytotoxic lymphocytes (TICLs), which are in the KT model. The Monte-Carlo approach employs the PCA rules, as in the models of Smolle and Stettner [4] and Conolly and Kimbell [27].

The paper is organized as follows: A phenomenological description of the tumor-immune interaction, and the method of the CA model are presented in Section II. In Section III, we present the simulation results for tumor progression. Then, insection IV, we compare the simulated results with the in vivo experimental results and find that the two are inagreement in many respects. For instance, the average growth curve of a thousand tumors simulated by our model agrees well with the Gompertzian growth curve of Ehrlich mouse carcinomas and spontaneous mouse carcinomas (C3H) as reported by Steel [41]. Also, the tumor morphology show that mainly proliferating cells are located at the outermost region of a tumor and that the fractality of the tumor boundaries agree well with the clinical experimental results of Bru et al. [20,42]. A computational investigation was performed to determine the qualitative growth curves for the dynamics for various value of each parameter in a sensitivity analysis, as discussed in Section 4, and some biological implications are given. In Section 5, several conclusions and a discussion are given.

II. OUTLINE OF THE CA MODEL

1. Model Design Rationale

It is well established that the immune system plays an important role in the growth of avascular tumors. Since the dynamics of the antitumor immune response in vivo is very complicated, following Matzavinos and Chaplain [10] we make a biological assumption about the tissue of a small multicellular tumor. The tumor-infiltrating cytotoxic lymphocytes (TICLs) have an element of random motility, so the kinetic model focuses on the attack on tumor cells by TICLs without necrosis and at the stage prior to (tumor-induced) angiogenesis.

According to the clinical studies in Matzavinos and Chaplain [10], "the tumor development can be effectively eliminated by tumor-infiltrating cytotoxic lymphocytes (TICLs) during the avascular stage. The TICLs may be cytotoxic lymphocytes (CTLs, CD8⁺ cells), natural killer-like (NK-like) cells, and/or lymphokine-activated killer (LAK) cells, including the cytostatic/cytotoxic activity of granulocytes and monocytes/macrophages lymphokine activated in the tumor." The TICLs can interact with the tumor cell, forming lymphocyte-tumor-cell complexes. The detachment results in the proliferating tumor cells dying due to programmed lysis or or escaping due to immune surveillance [10,44].

The escape mechanism that prevents the activation of the immune system has been studied by Anichini and Morarini [44]. One of the reasons for the escape result is that the cancer cells shed the antigen peptides on their surfaces, and by releasing blocking factors, which

$$P \xrightarrow{r'_{prolif.}} 2P$$

$$P + TICLs \xrightarrow{r_{binding}} C \xrightarrow{r_{lysis}} D + TICLs$$

$$D \xrightarrow{r_{decay}} .\phi$$

Fig. 1. Fundamental features of the development of cancer with an immune response (modified from Jain [37] and Matzavinos and Chaplain [10].

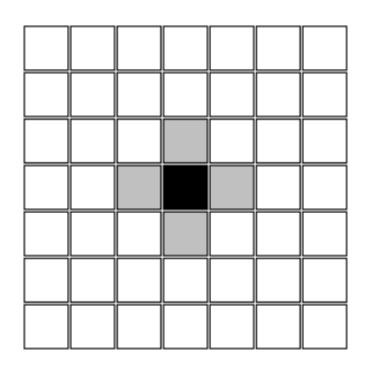


Fig. 2. Four nearest-neighboring sites (gray) of the tumor site (black) and the Nearest-neighbor rule (the so-called von *Neumann* neighborhoods).

can neutralize NK cells [37], they can decrease the efficiency of cytotoxicity behavior of immune activations [34]. A decline of the proliferation rate with increasing proliferation-tumor-cell numbers is assumed in the case of avascular microscopic tumor growth *in vivo* [20, 34, 41, 44, 45]. We will address these facts as fundamental assumptions to the model.

2. Fundamental Feature of Cancer Development With an Immune Response

The mathematical function [1] $r'_{prolif.}(t) = r_{prolif.} \left(1 - \frac{P}{K}\right)$, as an $in\ vivo$ avascular tumor growth rate, where P(t) is the number of proliferating tumor cells and K is the carrying capacity for tumor proliferation, has been defined. Simply speaking, the proliferation rate includes the crowding effect of viable tumor cells. As is evident, $r'_{prolif.}$ decreases when there is an increase in the number of proliferating malignant tumor cells. This will affect the first output of the first reaction as shown in Fig. 1 or Fig. 3. Moreover, the parameter $r_{prolif.}$ could indicate the proliferative activity of tumor cells. The definition of the rate of avascular tumor growth $in\ vivo$, $r'_{prolif.}$, may arise from

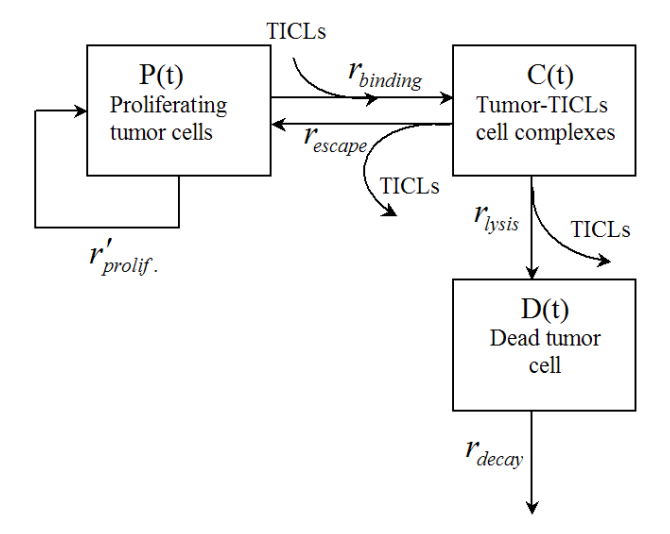


Fig. 3. Schematic diagram illustrating how cells in the tissue may change their state from one to another, and how cancer cells reproduce. P(t) denotes the number of proliferating cells at time t, C(t) denotes the number of TICLs-tumor cell complexes, and D(t) denotes the number of dead tumor cells. In this model, the function r'_{prolif} depends on the number of proliferating cells and on the carrying capacity of the proliferating cells.

limitation on the amount of nutrient that is available for the proliferation of cancer cells or from increasing accumulation of waste products, which causes a decrease in the proliferation rate of cancer cells [20,44].

In the second reaction, which we may call the cytolysis reaction, the parameter $r_{binding}$ is a measure of the recognition or response of TICLs to the proliferating tumor cells. The parameter r_{escape} describes the potential for the tumor escaping the host's immune surveillance [10,44]. The parameter r_{lysis} describes the potential for the immune system to deliver lethal hits to a tumor cell or to program a tumor cell's death [10,23,26,27,35].

For the last reaction, we introduce the parameter rdecay r_{decay} , which describes dissolution or disappearance of the dead cancer cells from the tumor (although, there is no definitive experimental data on the details of this tumor-cell destruction, a few authors have used this parameter [1,4,14,23,26,28,37,41].

According to the description above we denote the proliferating tumor cells, the dead tumor cells, the tumor infiltrating cytotoxic lymphocytes and the TICLs-tumor cell complexes by $P,\ D,\ TICLs,$ and C, respectively. The fundamentals of tumor development are schematically represented in Fig. 1.

The parameters $r_{prolif.}$, $r_{binding}$, r_{escape} , r_{lysis} , and r_{decay} are non-negative kinetic constants. $r_{prolif.}$ is the constant proliferation rate of tumor cells. $r_{binding}$ is the constant binding rate of TICLs to tumor cells. r_{escape} is the constant detachment rate of TICLs from cancer cells without damage to the cells. r_{lysis} is the detachment rate of TICLs from dead tumor cells due to the irreversible

programming of the tumor cells for lysis. The parameter r_{decay} is the constant decay rate of dead tumor cells.

The fundamental kinetics of tumor growth is transferred to the PCA rules in the same way as done by Qi et al. [1]. After setting of PCA rules, we use a computer program to implement the cell dynamics by using stochastic processes. A flowchart of the Monte Carlo simulation algorithm is given in Appendix A.

We now describe this automata-based model in more detail. The host tissue is represented as a lattice of size $L \times L$. In the tissue model, the coordinates (x_n, y_n) with $n = 1, 2, 3, \dots, L$ are designated by different values to indicate either normal cells, proliferating tumor cells, viable cells, cell complexes, or dead tumor cells. L is chosen to be sufficiently large so that the tumor cells never reach the boundary of the lattice, and there is no finite-size effect.

Time increases in discrete steps with synchronous updating, implying that in each time step, any site can be updated only once. We distinguish each tumor cell according to two possible states:

- [1] Proliferating state (*i.e.*, cancer or proliferating tumor cell, P), and
- [2] non-proliferating state or stationary state (i.e., C and D).

Each simulated tumor progresses according to the following algorithm:

- (I) At the initial time step, t=0 we start with an initial configuration of five cancer cells located at the center of normal tissue as shown in Fig. 2.
- (II) At each subsequent time step the rules of the cellular automaton are applied to each tumorous cell with the cells being randomly selected one by one with the same probability when the same cell type the same rates are used. A randomly selected cell will carry out one of the actions upon its state as shown in the schematic diagram, Fig. 3, as follows:
 - (1) Proliferating state: If the selected cell is a cancer cell, the cell has one of three possible actions with the function r'_{prolif} and the parameter $r_{binding}$.
 - (i) The cancer cell may invade a normal cell with a probability r'_{prolif} if the cancer cell has at least one nearest-neighbor normal cell randomly chosen with the same probability,
 - (ii) The cancer cell is bound by TICLs with a probability $r_{binding}$,

- (iii) The cancer cell may not change with a probability $1 (r'_{prolif.} + r_{binding})$ or there is no nearest neighboring normal sites in the case of invasion (probability $r'_{prolif.}$).
- (2) Stationary state: If the selected cell is in a non-proliferating state, which consists of dead cancer cells and TICL-tumor complex cells, which may be defined as cell complexes, it is a dead cancer cell or a TICL-tumor complex cell (now called a cell complex).
- (2.1) The complexes: The cell may take one of three actions with parameters r_{escape} , $r_{binding}$, and r_{lysis} :
 - (i) The complexes revert to a cancer cell with a probability r_{escape} ,
 - (ii) The complexes may lysis to a dead cancer cells with a probability r_{lysis} ,
 - (iii) The complexes may not change state with a probability $1 (r_{escape} + r_{lysis})$
- (2.2) The dead cancer cell: The site occupied by this dead cell may take on one of two actions according to parameter r_{decay} :
 - (i) The site may be reoccupied by a normal cell with probability r_{decay} ,
 - (ii) The cell may not change with probability $1 r_{decay}$,

All cells are selected, as in a time step.

(III) The PCA' rules (step II) are then applied iteratively to each time step until we reach a designated maximum number of time steps.

A pseudo-random number (r) is a part of a sequence generated by using a seed number supplied with a value in the range 0 < r < 1, The probabilities of various events are distributed in the interval 0 to 1. That is, the sum of the probabilities of actions in each cancer cell has to less than one. For implementation of the rules for cancer cells, the setting parameters have to satisfy $r_{prolif.} + r_{binding} \le 1$. Also, the setting parameters concerning the TICL-tumor-cell complexes have to satisfy $r_{escape} + r_{lysis} \le 1$.

III. SIMULATED RESULTS AND DISCUSSION

We have written a program to carry out the instructions given in the flowchart in Appendix A. The total number of tumor cells present at time t is denoted by N(t), which is equal to the sum of P(t), the number of proliferating tumor cells at time t, C(t), the number of TICL-tumor cell complexes at time t, and D(t), the number of dead tumor cells at time t; that is, N(t)

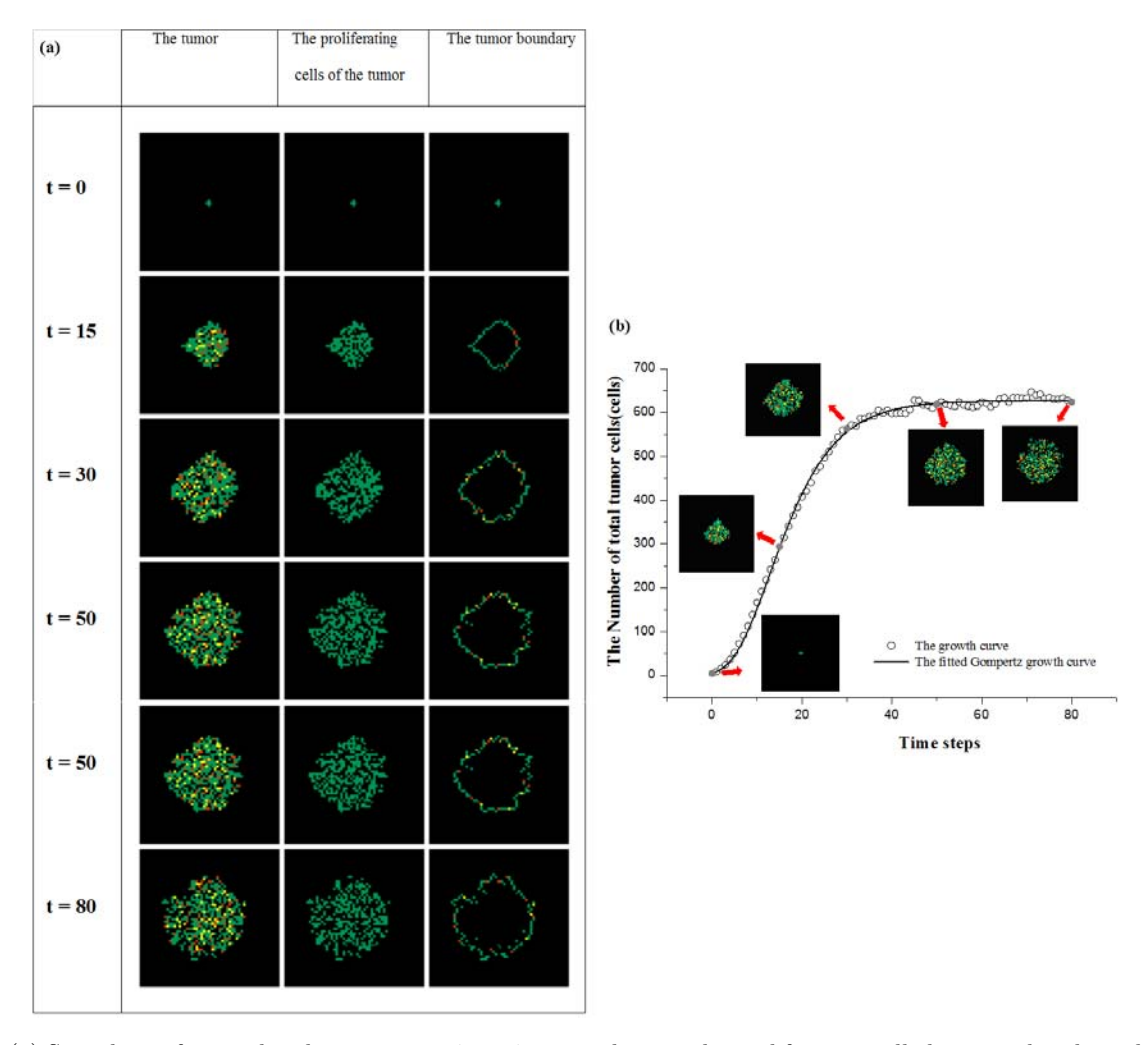


Fig. 4. (a) Snapshots of a simulated tumor on a 57 × 57 square lattice, the proliferating cell cluster and its boundary in time steps of 0,15, 30, 50, and 80, respectively. The simulation setting is $r_{prolif.} = 0.85$, $r_{binding} = 0.1$, $r_{escape} = 0.5$, $r_{lysis} = 0.35$, $r_{decay} = 0.35$, and K = 550. The color code is \square : proliferating tumor cell, \square : TICLs-tumor cell complexes, \square : dead tumor cell, and \square : normal cell. The definition of boundary cells for this model is a set of the outermost cells in each row and column of the two-dimensional square lattice. (b) Typical simulated tumor growth curve (circles) with the fitted Gompertz growth function. This fitting used the Gompertz parameters $A = 0.59363 \pm 0.00302$ and $B = 0.12285 \pm 0.00067$ with $r^2 = 0.99838$. This is the same simulation as in Fig. 4(a). The five snapshots of the simulated tumor at time steps of 0, 15, 30, 50, and 80 (solid gray) show the progression of the tumor shape.

P(t) + C(t) + D(t). Consequently, N(t) is the total number of tumor cells within a tumor, a measure of the size of the tumor at time t. We then average N(t) over Ts tumors, where N(t) is the total number of tumor cells in the tumor, and Ts is the number of tumors that are simulation.

The simulation is started by placing five tumor cells in the center of a square lattice. We then start the invasion of the tumor cells into the rest of the lattice, which represents normal tissue, by following the steps given in the algorithm of Section II.3. During a time step, we use a random number generator to choose the action that is to be taken by the cell, as detailed in Fig. 3. After a time step, the simulated results are obtained and a snapshot of the simulated tumor pattern at time t, as shown

in Fig. 4(a). Several two-dimensional illustrations of tumor invasion into normal, tissue as generated by the program, are shown in Figs. 4(a), 4(b), and 6(a).

1. Snapshots of a tumor and Its Growth Curve: Gompertz Growth Function

Some typical snapshots of the simulated tumor generated at different times are seen in Fig. 4(a). Fig. 4(b) shows the growth curve of this tumor growth with a fitted Gompertz function. The proliferation function of tumor cells and the related growth curve are shown in Fig. 5(a). The growth curves of tumors are shown, to-

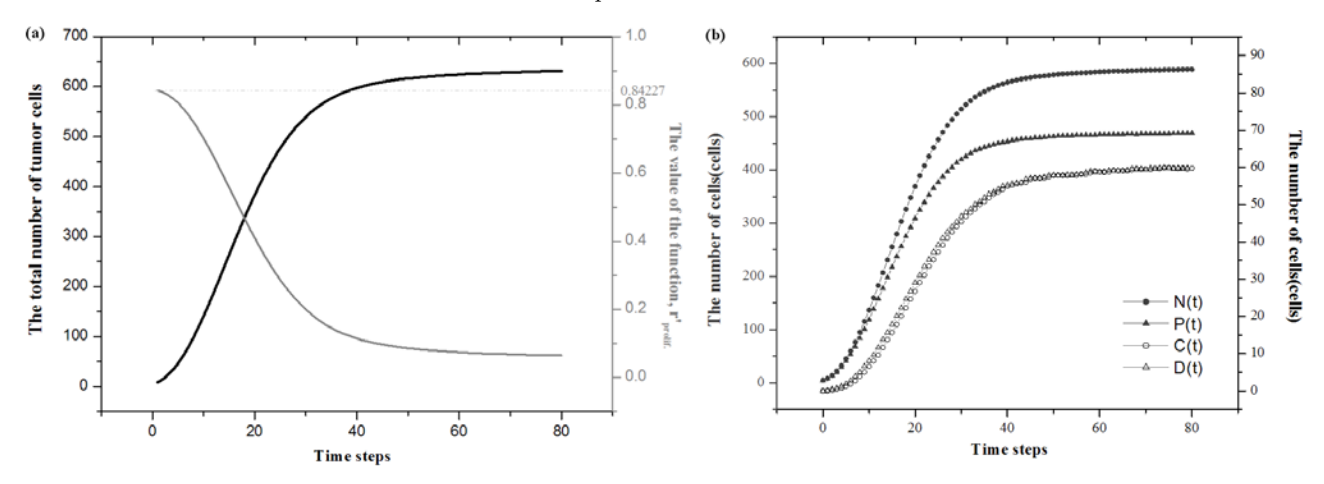


Fig. 5. (a) Plots of time evolutions of both the proliferating function value of avascular tumor growth, r'_{prolif} (gray solid line) and the total number of tumor cells (black solid line) from averaging 1000 simulated tumors. The proliferation rate of tumor cells in vivo is defined by $r'_{prolif} = r_{prolif} \left(1 - \frac{P}{K}\right)$, when P is the number of proliferating cells in the tumor, and K is the carrying capacity of the proliferating cells. We use the right axis for the functional value of r'_{prolif} and the left axis for the total number of tumor cells. The parameter settings are the same as in Fig. 4(a). (b) Time evolutions of the total number of tumor cells (gray solid circles), the number of proliferating cells (gray solid triangles), and the number of TICLs-tumor cell complexes (black triangles) and dead tumor cells (black stars). The averaged 1000 individual simulations use the same parameters as in Fig. 4(a).

Table 1. Summary of functions and constant input parameters for the model.

Function in the model	
$r'_{prolif.}$	Rate of proliferation of cancer cells (varies with the number of proliferating tumor cells)
Parameters	
$r_{prolif.}$	Base rate of proliferation of cancer cells
$r_{binding}$	Rate of TICLs binding with tumor cells form cell complexes
r_{escape}	Rate of breaking TICLs detachment from complex cells without damaging tumor cells
r_{lysis}	Rate of TICLs detachment from the complex cells as a result of the lysis of tumor cells
r_{decay}	Rate of dead tumor cells being degraded to normal cells
K	The carrying capacity of tumor proliferation

^{*} More extensive discussions of the parameters $r_{prolif.}$, $r_{binding}$, r_{lysis} , and r_{decay} are given by Lefever and Erneaux [23] and Qi et al. [1] while more extensive discussions of r_{escape} and r_{lysis} are given by Matzavinos and Chaplain [10]. The experimental data of $r_{binding}$ and r_{lysis} are given in Lefever and Erneux [59].

Table 2. Fitted Gompertz function fit to the growth curves of P(t), C(t), and D(t) of Fig. 5(b).

The type of cell in the tumor	A	В	Initial number of cells	Maximum	r^2
				number of cells	
Proliferating cell	0.54588	0.00106	5	469.697	0.99977
TICLs-cancer cell complexes	0.50530	0.10538	0.493	59.755	0.99969
Dead tumor cells	0.58502	0.10023	0.175	59.913	0.99948

gether with their constituent parts (proliferating cells, cells complexes, and dead tumor cells), in Fig. 5(b).

2. Growth Fraction Function and Growth Curve

The proliferation rate in vivo, r'_{prolif} , is the rate function due to the number of proliferating tumor cells in each time step, as represented in Fig. 5 for the same

parameter settings as Fig. 4(a). Fig. 5(a) shows the time evolutions of the total number of tumor cells (black solid line; left axis) and the evolution of r'_{prolif} (gray solid line, right axis). The rate r'_{prolif} gives the same behavior as reported by Gyllenberg and Webb [31]. Their was a function of the total number of tumor cells, but r'_{prolif} in our model is a function of the ratio of the number of proliferating cells to the total number of tumor cells. The growth fraction with the same trend

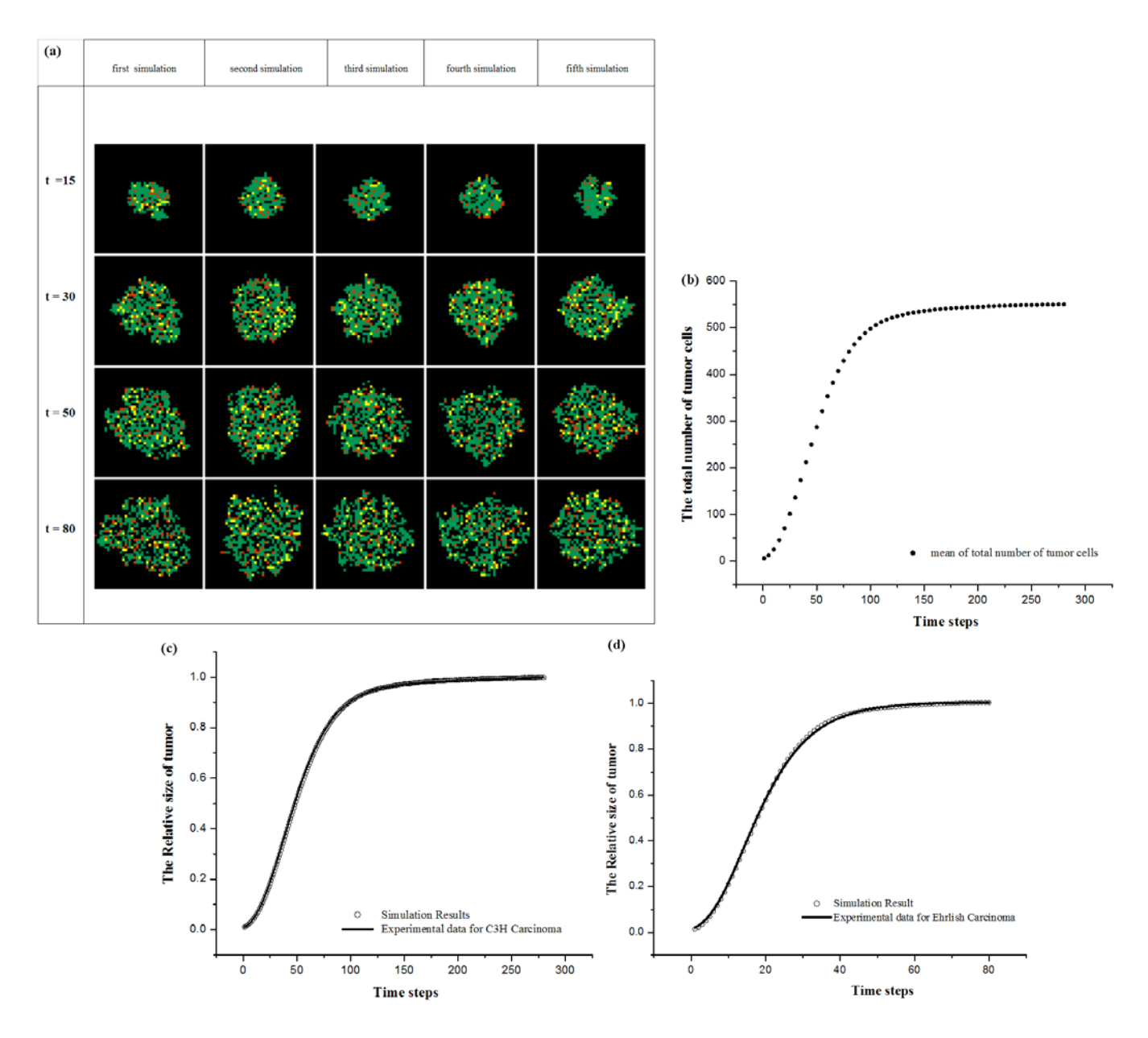


Fig. 6. (a) Influences of different series of pseudo-random numbers from five different seeds on the tumor shape on 47×47 square lattices with time progression for the same simulation settings as in Fig. 4(a). (b) Typical averaged growth curve, where the error bars are of the same magnitude as the size of the points. The simulation result is for an average over 1000 individual simulations with the parameters $r_{prolif.}=0.25$, $r_{binding}=0.04$, $r_{escape}=0.6$, $r_{lysis}=0.3$, $r_{decay}=0.35$, and K=550. (c) Comparison between the simulated tumor growth (circles) and the experimental growth curves in vivo for the spontaneous mouse carcinoma C3H (Steel [41] black solid line) with a coefficient of nonlinear regression $r^2=0.99985$. The Gompertz parameters are $V_o=0.0376$ (cm)³, A=0.177 (day)⁻¹, B=0.0311 (day)⁻¹, and $V_{max}=11.12$ (cm)³. The parameter settings are $r_{prolif.}=0.25$, $r_{binding}=0.04$, $r_{escape}=0.6$, $r_{lysis}=0.3$, $r_{decay}=0.35$, and K=550 with $N_o=6.02$ and $N_{max}=551.18$. (d) Comparison between the simulated tumor growth and the experimental growth curves in vivo for mouse Ehrlich [41] carcinoma with the coefficient of nonlinear regression $r^2=0.9997$. The Gompertz parameters are $V_o=0.0226$ (cm)³, A=0.456 (day)⁻¹, B=0.102 (day)⁻¹, and $V_{max}=1.94$ (cm)³. The parameter settings are $r_{prolif.}=0.85$, $r_{binding}=0.1$, $r_{escape}=0.5$, $r_{lysis}=0.35$, $r_{decay}=0.35$, and K=550 with $N_o=8.381$ and $N_{max}=627.379$.

as that of two-compartment cell-population model of Gyllenberg and Webb [31] also revealed Gompertzian growth.

IV. COMPARISON OF SIMULATION RESULTS WITH EXPERIMENTAL RESULTS

A spatial visualization of tumor spreading on the twodimensional square lattice leads us to some results: The growth curve from simulation in good agreement with experimental data for Ehrlich mouse carcinomas and for spontaneous mouse carcinomas (C3H) as reported by Steel [41]. The fractality of the boundary, the spatial distribution of cell proliferation, and the relevant biological implications will be represented.

1. Snapshots of Five Typical Simulated Tumors and the fractality of the boundary

The different morphologies of five typical simulated tumor patterns are shown in Fig. 6(a). Fig. 6(b) shows the growth curve for an average of over 1000 realizations.

The tumors obtained from the stochastic model are found to have an approximately circular shape with a rough boundary, as shown in Fig. 3(a). A few researchers [6-8,19,46-48] have been interested in the fractal dimension (D_f) of the stochastic growth model. We define the boundary cells of the simulated tumor using assuming that they are the outermost cells of the tumor in each row and each column in the lattice. The irregular boundaries of tumors can be examined by using a fractal geometric analysis. Moreover, the concept and measurement of fractal dimension by using the box-counting method is given by Bru et al. [20], Cross [49], Laird [50]. Malignant melanomas in vivo have been investigated and the fractal dimension of the boundary of the tumor is found to lie mainly in the range 1.05 - 1.30 [49]. Bru, et al. [20] and also published in vitro and *In-vivo* experimental data for the boundary of human and animal solid tumors with values of D_f in the range of 1.09 - 1.34, which agrees well with the data of Cross [49]. Our mean fractal dimension of five tumor boundaries (between time steps 10 and 350) lies in 1.11 - 1.22, which agrees well with the observations of other researchers Bru et al. [20], Lefever and Erneux [23], and Cross [49]. The fluctuating boundary of a simulated tumor can be show to have nearly the same shape as the boundary of tumors in clinical studies.

2. Comparisons of the Average Growth Curve with the Experimental Data

The Gompertz growth curve is the most commonly used curve to fit the experimental data for *in-vivo* tumor

growth [40,41,50,51] and is an important feature noticed in actual tumor growth. The Gompertz curve [41,52,53] is given as

$$V(t) = V_o \exp\left\{\frac{A}{B}(1 - \exp(-Bt))\%\right\},\tag{1}$$

where V(t) is the size of the tumor at time t, V_o is the initial size, and A and B are two positive parameters whose values are determined by a least-square best fit of Eq. (1) to the data. Fig. 6(a) shows the average growth curve of a thousand tumors. At time t tumor i will give $N_i(t)$, with the error bar for Ts tumors being defined as $2\sqrt{\frac{\sum_{i=1}^{Ts}(N_i(t)-\bar{N}(t))^2}{Ts-1}}$ at the 95 % confidence interval. Fig. 6(b) represents the averaged growth curve from

1000 simulation runs with their error bars having the same magnitude as the data points. The averaged growth data from our simulation runs with settings $r_{prolif} = 0.25, r_{binding} = 0.04, r_{escape} = 0.6, r_{lysis} =$ 0.3, $r_{decay} = 0.35$, and K = 550 is shown in Fig. 6(c). It is noteworthy to note that the Gompertz curve was used to fit the experimental growth curve of tumors in vivo. The Gompertz parameters for the experimental data for a spontaneous mouse carcinoma (C3H) are $V_o = 0.0376$ $(cm)^3$, $A = 0.177 (day)^{-1}$, $B = 0.0311 (day)^{-1}$, and V_{max} $= 11.12 \text{ (cm)}^3$. To obtain the fit, we had to normalize both the simulation and the experimental data. The normalization of the Gompertz curve was such that the maximum size and the normalization of the simulated data was, respectively, $N_o = 6.02$ and $N_{max} = 551.18$. The two normalized growth curves are shown together in Fig. 6(c).

The averaged growth curve yielded by our simulation runs with settings $r_{prolif} = 0.85$, $r_{binding} = 0.1$, $r_{escape} = 0.5$, $r_{lysis} = 0.5$, $r_{decay} = 0.5$, and K = 550 is shown in Fig. 6(d). The Gompertz parameters for the experimental data of Ehrlich carcinomas in mice are $V_o = 2.26 \times 10^{-7} \text{ (cm)}^3$, $A = 0.456 \text{ day}^{-1}$, $B = 0.102 \text{ day}^{-1}$, and $V_{max} = 1.94 \text{ cm}^3$. The normalization of the simulated data was such that $N_{max} = 625$ and $N_o = 8.394$. The two normalized growth curves for Ehrlich carcinomas are shown together in Fig. 6(d).

${\bf 3.} \ \ {\bf Spatial \ Distribution \ of \ proliferated \ Cell \ in}$ ${\bf tumors}$

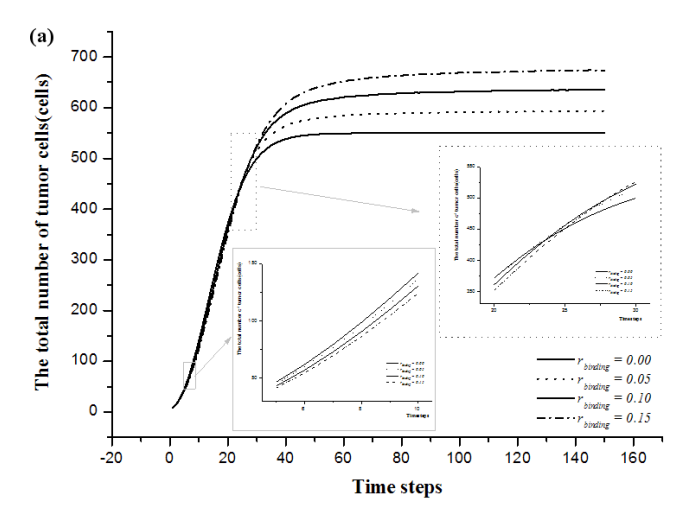
Bru et al. [20], clinically studied the spatial distribution of cell proliferation in tumors by counting after tracking with Bromodeoxyridine (Brdu). In particular, Bru et al. [20] defined three regions of the avascular tumor on the basis of the radius of the tumor (assuming that the tumor is circular). The innermost region lies in the region $0 \le r_i < R/2$. The intermediate region lies in the region $R/2 \le r_i < 4R/5$. Finally, the outermost region lies in the region $r_i \ge 4R/5$. r_i is the distance of a particular site occupied by a cancer cell from the center

of the tumor. They measured the number of proliferating cells in each of the three regions in a human colon adenocarcinoma. They found that the innermost region contained 6 % of the proliferating cancer cell and made up 25 % of the tumor. The intermediate region contained 14 % of the proliferating cells and made up 39 % of the tumor. The last region contained 80 % of the proliferating cells and made up 36 % of the tumor. Most of the proliferating cells were found in the outermost regime, similar to that found by Bru et al. [20]. The ratio of proliferating cancer cells found in the three regions is 80 : 14:6 (in order of outermost to innermost). Fig. 4(a) has shows the proliferating cells in a typical tumor. We measured these quantities by averaging over 1000 simulated tumors with parameters $r_{prolif} = 0.85, r_{binding} =$ $0.1, r_{escape} = 0.5, r_{lysis} = 0.35, r_{decay} = 0.35, \text{ and } K$ = 550. We empirically set the saturation phase of the tumor growth from time steps 80 to 150 and the ratio of proliferating tumor cells that we found for the outermost, intermediate, and innermost regimes, was 71:17:11. The errors were 0.094, 0.082, and 0.124, respectively. We may conclude that the proliferating cells of the simulated tumor were located mostly in the outermost regions.

4. Sensitivity Analysis by Varying parameters with Some Biological Effect

We changed the values of some of the parameters in the model to see how the growth of the tumor would be affected. The ranges chosen for the parameter values in our model were motivated either by experimental clinical data [1,23] or by the computational experiment results Steel [41], and Barabasi and Stanley [51]. All simulation results could be fitted well with a Gompertz function.

Mathematically, the behavior of the Gompertz curve can be divided into three regions [53]. These are determined by the position of the inflection point [41], and the crossover time [51]. Biologically speaking, the three regions reflect different growth behavior. The first region or early phase reflects the dynamics of the initial stage of tumorigenesis. The phase continues until the number of tumor cells reaches a value equal to 0.37 of the maximum number of tumor cells. The time step at which this occurs is called the infection point in the curve. We denote this time as t_1 . The second region or intermediate phase of the growth curve is the portion of the curve which begins at t_1 and extends to the crossover point at t_2 . The crossover point is the intersection of the tangent lines of the initial portion of the Gompertz curve and of the saturated part of the Gompertz curve. Then, the time t_2 means the time to reach the saturated phase of the Gompertz curve. The third region of the curve starts at the cross over point and extends into the saturated state. The three regions of the Gompertz curve are shown in Appendix B.



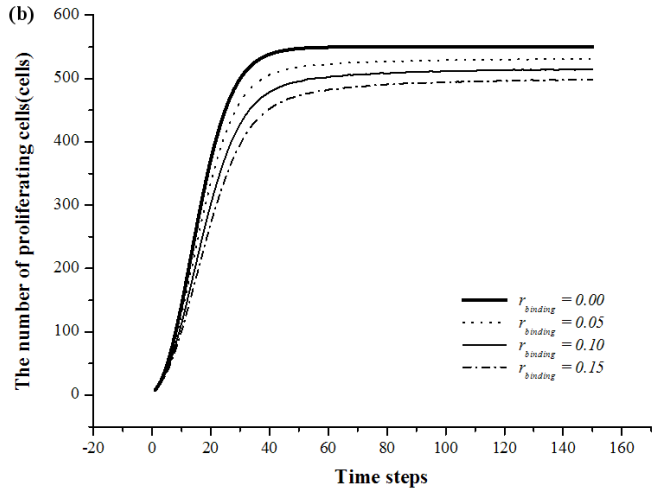


Fig. 7. (a) Plots of the time evolution of the total numbers of tumor cells. The inset shows magnified time step of 5 to 10 and 20 to 30. The simulation results are averaged over 1000 individual realizations by varying the value of $r_{binding}$ from 0.00 to 0.15 in steps of 0.05 while fixing the other values at $r_{prolif.}=0.85,\,r_{escape}=0.5,\,r_{lysis}=0.35,\,r_{decay}=0.35,\,{\rm and}\,K=550.$ (b) Plots of the time evolutions of the numbers of proliferating cells. The simulation results are averaged over 1000 individual realizations with the same parameters as in Fig. 7(a).

To see how the immune system influences the growth of the tumor, we varied $r_{binding}$ and r_{escape} because the value of these two rates depends on the immune system. We varied the value of $r_{binding}$ and obtained the simulation results as shown in Figs. 7(a), and 7(b). We can conclude that the proliferating cells decrease as the rate of binding with TICLs increases. This also causes saturation to be reached at a later time.

The escape rate reflects the efficiency of cancer cells evading the binding process of TICLs. A greater escape rate indicates a shorter time for binding maintenance before cancer cells evade unfolding TICLs. We varied r_{escape} to get the simulation results shown in Figs. 8(a),

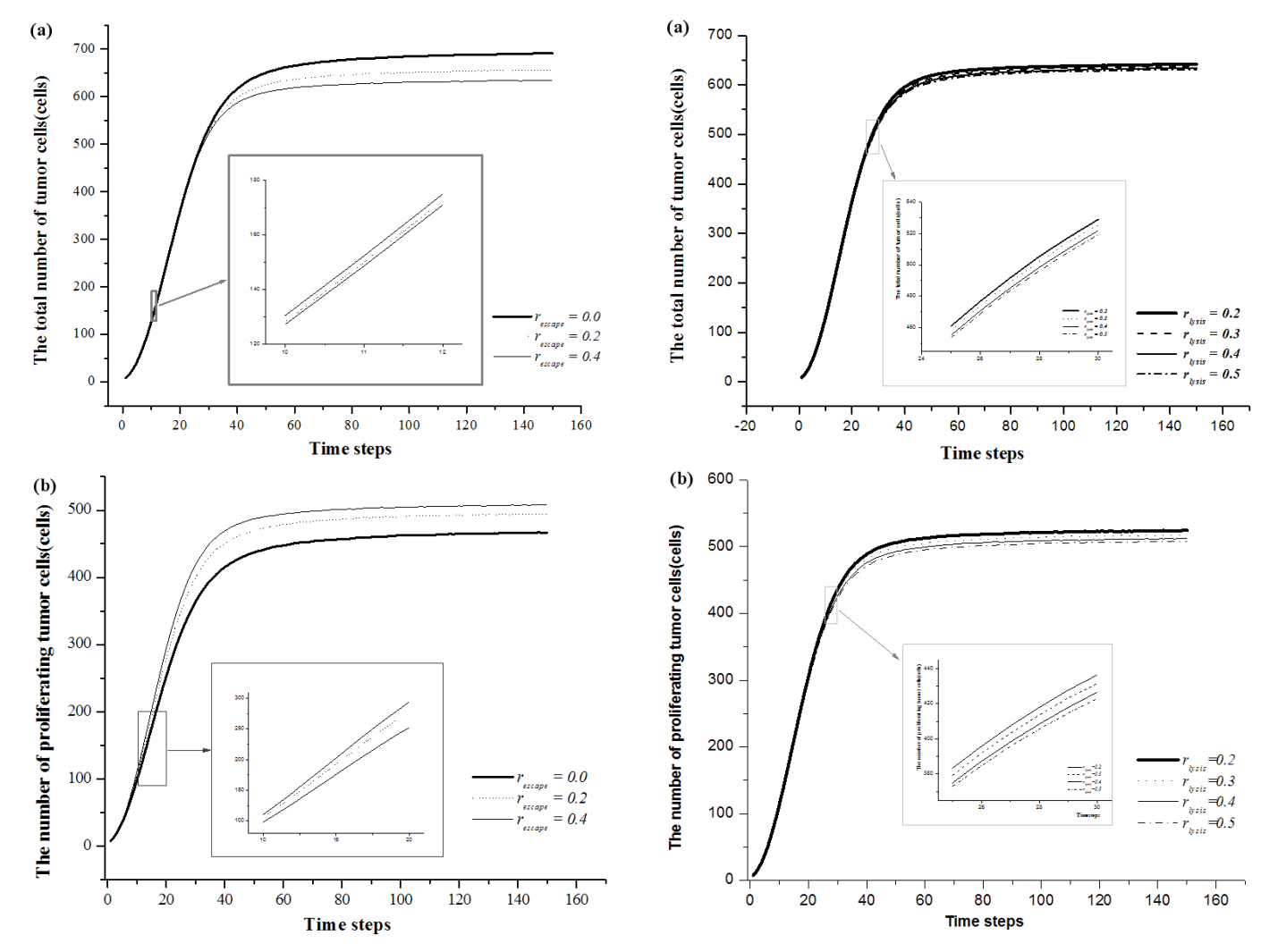


Fig. 8. (a) Plots of the time evolution of the total number of tumor cells. The simulation results are averaged over 1000 individual realizations by varying the value of r_{escape} from 0.0 to 0.4 in steps of 0.2 while fixing the other values at $r_{prolif.} = 0.85$, $r_{binding} = 0.1$, $r_{lysis} = 0.35$, $r_{decay} = 0.35$, and K = 550. (b) Plots of the time evolutions of the total number and the number of proliferating tumor cells of the simulated tumor. The simulation results are averaged over 1000 individual realizations with the same parameters as in Fig. 8(a).

Fig. 9. (a) Plots of the time evolution of the total number of tumor cells. The simulation results are averaged over 1000 individual realizations by varying the value of r_{lysis} while fixing the other values at $r_{prolif.} = 0.85$, $r_{binding} = 0.1$, $r_{escape} = 0.5$, $r_{decay} = 0.35$, and K = 550. (b) Plots of the time evolutions of the total number and the number of proliferating tumor cells of the simulated tumor. The simulation results are averaged over 1000 individual realizations with the same parameters as in Fig. 9(a).

and 8(b). The growth curves for the proliferating tumor cells show that increasing r_{escape} will cause a rate of growth increase in the initial phase. Saturation will be achieved in a shorter time with a greater tumor size as r_{escape} increases.

The lysis rate, r_{lysis} , is the death rate of cancer cells due to programmed death. We varied the value of the parameter r_{lysis} and obtained the results shown in Fig. 9(a) and 9(b). The growth of the number of proliferating tumor cells increases only slightly with increasing r_{lysis} in the initial phase. The growth curves reach crossover

more they do for than smaller sizes. We found an essential difference concerning variation of the lysis rate between our model and that of Qi et~al.~[1]. The conclusion of Qi et~al.~[1] is that a greater r_{lysis} , gives a greater number of proliferating cells in the third region. We can get the same result as Qi et~al.~ do [1] without the escape mechanism.

The decay rate, r_{decay} , may be considered as the efficiency of TICLs in destroying the cancer cells with programming for lysis after unfolding. A greater decay rate yields a shorter time for destruction of cancer cells. r_{decay} was varied from 0.2 to 0.5 in steps of 0.1 with

the values of all the other parameters kept constant. Increasing the decay rate of the cancer cells resulted in a decrease in the total number of cancer cells and a slight increase in the number of proliferating tumor cells in the third region. The crossover point for each curve was be reached in a shorter time.

From our studies, it is yet to be seen if experimentalists can take advantage of our findings. After we have the simulational results for various parameters, it is worth discussing some biological implications of those results so that the biological impacts for some parameters might be understood. The biological meaning of each parameter is as follows:

- 1. The proliferative activity of tumor cells is reduced by decreasing r_{prolif} . Clinical trials have shown that increasing proliferation rates yield smaller tumors [31,54]. For instance, Blay et al. [54] studied gastrointestinal stromal tumors (GIST), which are solid tumors. GISTs exhibit typical activating mutations of KIT or PDGFRA proto-oncogene, which are most likely causal molecular events of GISTs. Oncogene-targeted therapy using Imatinib, a tyrosine kinase inhibitor blocking most mutatedactivated KIT and (platelet-derived growth-factor receptor) PDGFR α proteins of GISTs, controlled tumor growth up to 85 %. This therapy may lead to elimination of both new proliferating tumors and existing tumors. The parameters that affect adoptive therapy may decrease $r_{prolif.}$, and the comparison with our simulation results is good.
- 2. Ehe defensive activity of immune cells is modified by increasing $r_{binding}$ and r_{lysis} in order to have a faster response by the immune response system. Studying the many clinical experiments (1995-2001) of Matzavinos and Chaplain [11], we conclude that cytokines are one of the components of the immune system that are involved in modulating the local cellular immune response dynamics with the production of several interleukins (IL-2, IL-10, and IL-12), cell-adhesion molecules and chemokines in tumor tissue, the induced chemotaxis of T-cells, and the cytotoxic reactions of TICLs against tumor cells. Consequently, the effectiveness of cytokines might be the reason for increasing $r_{binding}$ and r_{lysis} in the kinetic model.
- 3. A modification of the aggressiveness of immune cells against the tumor by increasing the parameter r_{lysis} give a more efficient immune activity. Almost all breast cancer patients have hormone receptor positivity. Tamoxifen is a hormonal treatment for breast cancer. Hickman [55] has studied anticancer therapies by induced apoptosis. Ellis $et\ al.\ [56]$ have reported clinical studies that show that increases in apoptosis in human breast cancer occur with tamoxifen treatment. Dowsett $et\ al.\ [39,57]$, Cameron $et\ al.\ [40]$, and Bardon $et\ al.\ [58]$ studied

tumor regression in breast cancer xenografts with tamoxifen and have been reported the same results. Xenograft studies support increased apoptosis and decreased proliferation after oestrogen withdrawal [39]. However, the relative importance of these two processes still remains unclear [40].

We increased r_{lysis} with the other parameters fixed, which means that the escape parameter is also fixed. The kinetic model in Fig. 1 shows the competition between TICLs and cancer cells. Increasing r_{lysis} and fixing r_{escape} may yield enhanced immune efficiency, implying a decrease in the number of proliferating cells due to the escape process. If the rate r_{lysis} , is increased the dead cancer cells increase in number, which also decreases the quantity of escaping cancer cells from the TICL-cancer cell complexes, ultimately decreasing proliferation.

V. CONCLUDING REMARKS

The kinetic model shown in Fig. 1 shows a tumor growth that is governed by the processes of proliferation, binding, escape, lysis, and decay by using the cellular automaton method with five parameters to represent these processes. With this kinetic model and the simulation method, we can show that different sets of the five kinetic parameters will give differing Gompertzian curves.

We can conclude from the simulation results that a greater tumor size might not indicate aggressiveness of tumor growth. In particular, we agree with Steel [41] that the quantity of proliferating cells be a better indication of tumor size.

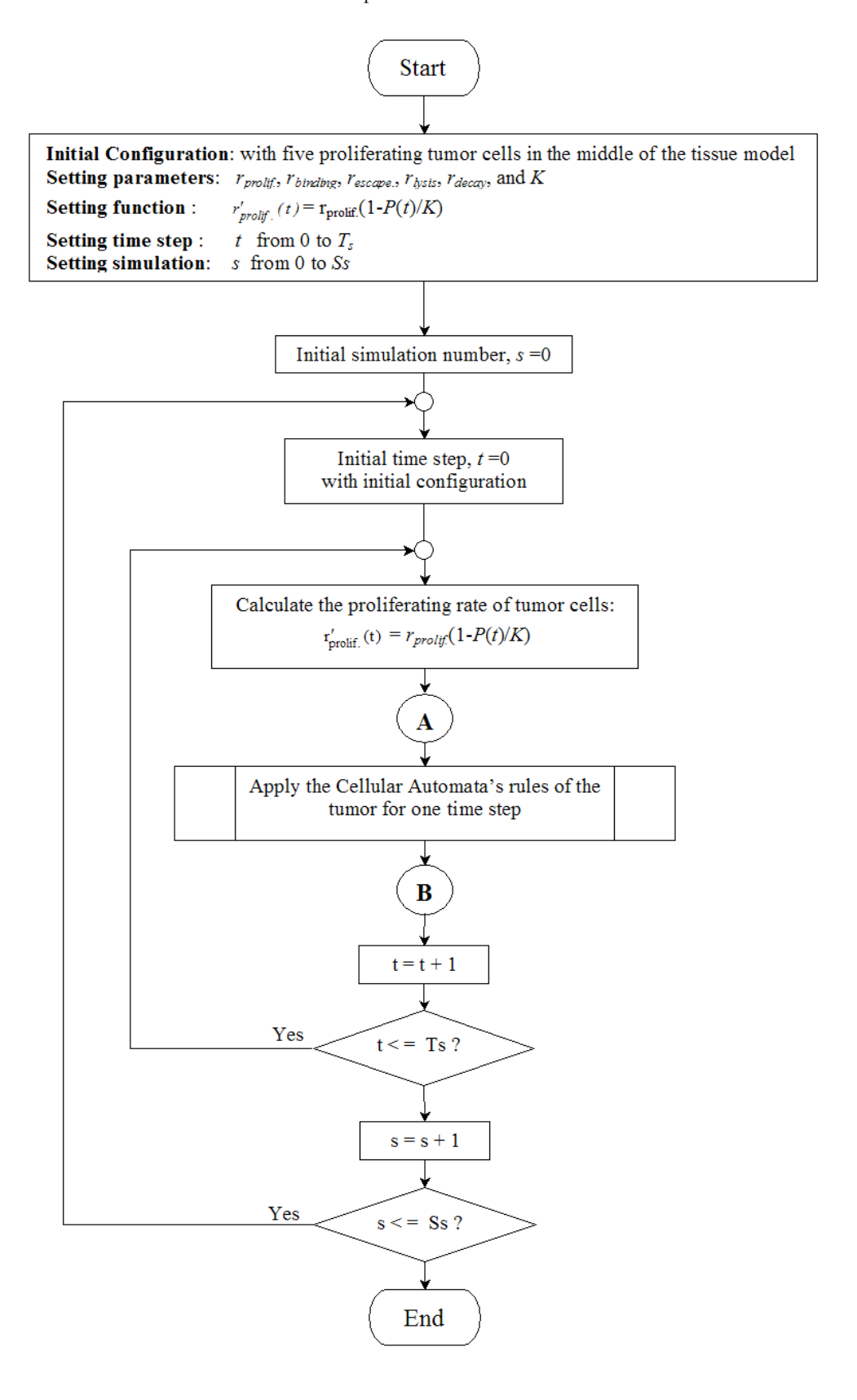
This CA model also allows us to quantify the proportion of each cell type within a simulated tumor as a function of each set of five parameters. The cellular automata model on a three-dimensional square lattice is also in the process of development.

APPENDIX A: FLOWCHART OF THE MONTE CARLO CELLULAR AUTOMATA ALGORITHM OF TUMOR

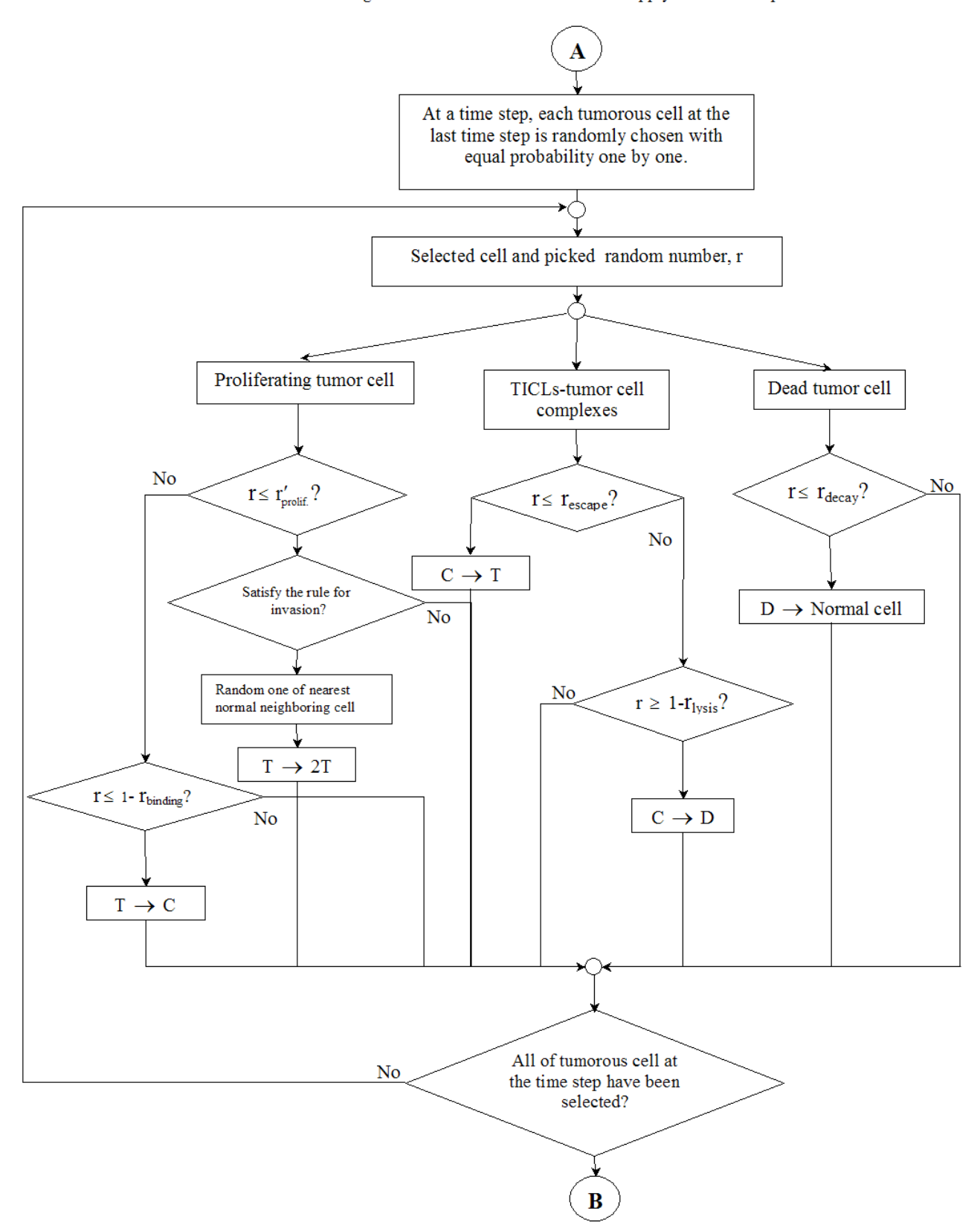
Initial Configuration : with five proliferating tumor cells in the middle of the tissue model

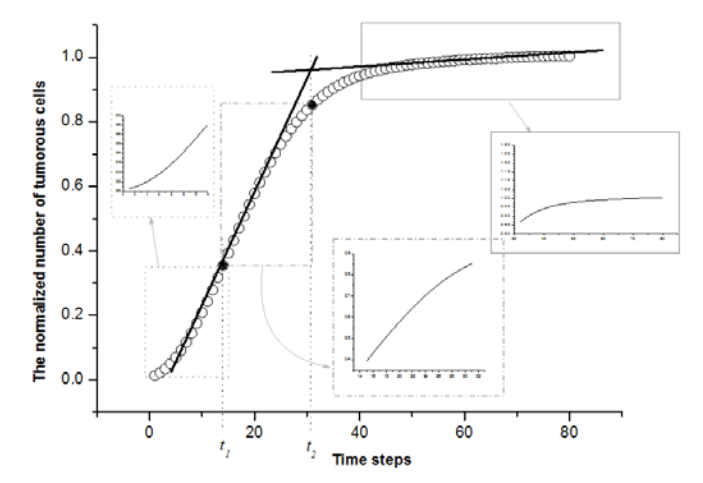
APPENDIX B

Plots of the time evolution of the total number of tumor cells (circles). The three segments of the sigmoidal Gompertzian curve from the simulation results show



The algorithm of cellular automata 's rule apply for a time step





different growth dynamics. The first segment has range from 0 to $14(t_1)$ time steps at the first solid circle; the second phase runs from day 15 until the time step at $31(t_2)$, that is the crossover time; the third phase begins at 32 days from the second solid circle. The simulation results are averaged over 1000 individual realizations with the simulation settings $r_{prolif.}=0.85,\ r_{binding}=0.1,\ r_{escape}=0.5,\ r_{lysis}=0.35,\ r_{decay}=0.35,\ {\rm and}\ K=550.$

ACKNOWLEDGMENTS

The authors would like to thank J. Poulter for his fruitful discussions and proofreading. One of the authors (A. B.) would like to thank T. J. Newman and the Department of Physics and Astronomy at Arizona State University for the training program in the US for one year (2003-2004), C. Quince who helped in improving programme development. T. Dhirasakdanon, and T. Sungkaworn who supplied relevant important papers. Additionally, we would like to thanke P. Kanthang, W. Ngamsa-ad, S. Chadsuthi, H. Pitakjakpipop, and C. Modchang who are in the biophysics group at Mahidol University, for their technical assistance with software support concerning. This research work was financially supported in part by Mahidol University, the Thailand Research Fund (TRF), the National Center for Engineering and Biotechnology, Thailand (BIOTEC), and the Institute of Innovation and Development of Learning Process.

REFERENCES

- A. S. Qi, X. Zheng, C. Y. Du and B. S. An, J. Ttheor. Biol. 161, 1 (1993).
- [2] A. R. Kansal, S. Torquato, G. R. Harsh, E. A. Chiocca and T. S Deisboeck, J. Theor. Biol. 203, 367 (2000).

- [3] A. R. Kansal, S. Torquato, G. R. Harsh, E. A. Chiocca and T. S Deisboeck, Biosystems. 55, 119 (2000).
- [4] J. Smolle and H. Stettner, J. Theor. Biol. 161, 63 (1993).
- [5] D. Kirschner and J. C. Panetta, J. Math. Bio. 37, 235 (1998).
- [6] Jr. S. C. Ferreira, M. L. Martins and M. J. Vilela, Physica A 261, 569 (1998).
- [7] Jr. S. C. Ferreira, M. L. Martins and M. J. Vilela, Physica A 271, 245 (1999).
- [8] M. V. Voitikova, arXiv:comp-gas/9811001, (1998).
- [9] J. Smolle, H. P. Soyer, F. M. Smolle-Juettner, H. Stettner and H. Kerl, Path. Res. Pract. 186, 467 (1990).
- [10] A. Matzavinos and J. Chaplain, Math. Med. and Bio. 21, 1 (2004).
- [11] A. Matzavinos and J. Chaplain, C. R. Biologies. 327, 995 (2004).
- [12] W. Duchting and T. Vogelsaenger, Int. J. Bio-Medical Computing 12, 377 (1981).
- [13] N. Bellomo and L. Preziosi, Mathl. Comput. Modelling 32, 413 (2000).
- [14] M. Galach, Int. J. Appl. Math. Comput. Sci. 13, 395 (2003).
- [15] T. Alarcon, H. M. Byrne and P. K. Maini, J. Theor. Biol. 225, 257 (2003).
- [16] N. Buric and D. Todorovic, Chaos, Solitons and Fractals 13, 645 (2002).
- [17] P. Daugulis, et al., Hopf bifurcation analysis for angiogenesis models, Discrete and Continuous Dynamical Systems, in press.
- [18] S. Habib, C. Molina-Paris and T. S Deisboeck, Phys. A 327, 501 (2003).
- [19] Y. Mansury and T. S. Deisboeck, Physica A 219, 219 (2004).
- [20] A. Bru, S. Albertos, J. L. Subiza and J. L. Garcia-Asenjo, Biophysic Journal. 85, 2948 (2003).
- [21] V. A. Kuznetsonov and M. A. Taylor, Bull. Math. Biol. 56, 295 (1994).
- [22] G. J. Pettet, C. P. Please, M. J. Tindall and D. L. McElwain, Bull. Math. Biol. 63, 231 (2001).
- [23] R. Lefever and T. Erneux, Plenum Publishing Corporation (New York, 1984).
- [24] A. A. Patel, E. T. Gawlinski, S. K. Lemieux and R. A. Gatenby, J. Theor. Biol. 213, 315 (2001).
- [25] A. Bru, S. Albertos, J. L. Subiza and J. L. Garcia-Asenjo, Phys. Rev. Lett. 92 23, 238101 (2004).
- [26] M. R. Owen and J. A. Sherratt, J. Theor. Biol. 189, 63 (1997).
- [27] R. B. Conolly and J. S. Kimbell, Toxicology and Applied Pharmacology 124, 284 (1994).
- [28] D. D. Dionysiou, G. S. Stamatakos, N. K. Uzunoglu and K. S. Nikita, Comp. in Bilol., Med. Article in press (2005).
- [29] D. Drasdo, R. Kree and J. S. McCaskill, Phys. Rev. E 52, 6635 (1995).
- [30] H. P. Greenspan, J. Theor. Biol. **56**, 229 (1976).
- [31] M. Gyllenberg and G. F. Webb, Growth, Dev. Aging 53, 25 (1989).
- [32] W. Sa-Nguansin, W. Triampo and N. Nattavut, J. Korean Phys. Soc. 46, 1429 (2005).
- [33] J. Wong-ekkabut, W. Triampo, D. Triampo, I. M. Tang and Y. Lenbury, J. Korean Phys. Soc. 45, 310 (2004).
- [34] A. Kataki, P. Scheid, M. Piet, B. Marie, N. Martinet, Y. Martinet and J.-M. Vignaud, J. Lab Clin. Med. 140,

- 320 (2002).
- [35] A. S. Perelson and G. I. Bell, J. Immunol. 129, 2796 (1982).
- [36] A. S. Perelson, L. S. Mackoos and B. Bonavida, V. Kinetics of (1984).
- [37] S. Jain, Cancer Cell Int. 2, 13 (2002).
- [38] G. C. Easty, G. C. Ambrose and F. J. Croe (Eltis Horwood Limited, 1975), p. 58.
- [39] M. Dowsett, C. Archer, L. Assersohn, R. K. Gregory, P. A. Ellis, J. Salter, J. Chang, P. Mainwaring, I. Boeddinghaus, S. R. D. Johnston, T. J. Powles and I. E. Smith, Endocrine-Related 6, 25 (1999).
- [40] D. A. Cameron, A. A. Ritchie and W. R. Miller, Eur. J. Can. 37, 1545 (2001).
- [41] G. G. Steel (Clarendon press, New York, 1977).
- [42] A. Bru, J. M. Paster, I. Fernaud, I. Bru, S. Melle, C. Berenguer, Phys. Rev. Lett. 81, 4008 (1998).
- [43] L. P. Preziosi, J. Immunol. **132**, 2190 (2003).
- [44] A. Anichini, G. Bevila cqua, R. Gavazzi and P. L. Lollini, Eds. (1995).
- [45] F. Kozusko and Z. Bajzer, Math. Bios. 185, 153 (2003).
- [46] P. F. Ho and C. Y. Wang, Math. Biosci. 155, 139 (1999).
- [47] S. Dormann, The Dessertation Zur Erlangung des Grades eines Doktors der Naturwissenschaften (2000).
- [48] C. Y. Wang and J. Bassingthwaighte, Math. Bio. 142, 91 (1997).
- [49] S. S. Cross, J. Pathol. **182**, 1 (1997),
- [50] A. K. Laird, Br. J. Cancer 19, 278 (1964).

- [51] A. L. Barabasi and H. Stanley (Cambridge University Press, Cambridge, 1995).
- [52] W. Mueller-Klieser, S. Schreiber-Klais, S. Walenta and M. H. Kreuter, Int. J. Oncol. 21, 1307 (2002).
- [53] L. Norton, R. Simon, H. D. Brereton and A. E. Bogden, Nature 264, 542 (1976).
- [54] J.-Y. Blay, S. Bonvalot, P. Casali, H. Choi, M. Debiec-Richter, A. P. Dei-Tos, J.-F. Emile, A. Gronchi, P. C. W. Hogendoorn, H. Joensuu, C. A. Le, M. J. Mac-Clure, J. Maurel, N. Nupponen, I. Ray-Coquard, P. Reichardt, R. Sciot, S. Stroobants, M. van Glabbeke and G. D. Demetri, Annals of Oncology 16, 566 (2005).
- [55] J. A. Hickman, Cancer Metastasis Rev. 11, 121 (1992).
- [56] P. A. Ellis, G. Saccani Jotti, R. Clarke, S. R. D. Johnston, E. Anderson, A. Howell, R. A'Hern, J. M. Salter, S. Detre, R. Nicholson, J. Robertson, M. Baum, I. E. Smith and M. Dowsett, International Journal of Cancer 72, 608 (1997).
- [57] M. Dowsett, S. R. D. Johnston, J. Newby, M. Golding, N. Sacks and I. E. Smith, Endoc-Relat Cancer 2, 3 (1995).
- [58] S. Bardon, F. Vignon, P. Montcourrier and H. Rochefort, Cancer Res. 47, 1441 (1987).
- [59] D. A. Cameron, A. A. Ritchie, S. Langdon, T. J. Anderson and W. R. Miller, Breast Cancer Research and Treatment 45, 99 (1977).
- [60] P. Waliszewski and J. Konarski, Chaos, Solitons and Fractals 16, 665 (2002).

A Simple Deterministic Model for the Spread of Leptospirosis in Thailand

W. Triampo, D. Baowan, I.M. Tang, N. Nuttavut, J. Wong-Ekkabut, and G. Doungchawee

Abstract—In this work, we consider a deterministic model for the transmission of leptospirosis which is currently spreading in the Thai population. The SIR model which incorporates the features of this disease is applied to the epidemiological data in Thailand. It is seen that the numerical solutions of the SIR equations are in good agreement with real empirical data. Further improvements are discussed.

Keywords—Leptospirosis, SIR Model, Deterministic model, Thailand.

I. INTRODUCTION

EPTOSPIROSIS, a worldwide zoonotic disease, is an acute febrile illness caused by pathogenic spirochete of the genus Leptospira [1,2]. The disease is considered to be a major public health problem worldwide. The illness resulting from the disease ranges from a mild flu-like illness to a severe or fatal disease involving renal and/or liver failures and (referred as Weil's syndrome) [3]. Most outbreaks tend to be seasonal in nature and are often linked to environment factors, to animals and to agricultural and occupational cycles like cultivating rice in marshy land. Mammals such as rats and cattle are commonly involved in exposure to contaminated tissues or urine [1,2,4]. Outbreaks of leptospirosis occur mainly after flooding, leading to its become an occupational hazard for sanitary and agricultural workers as well as being recreational hazard for humans [5]. Some pathogenic leptospires have been found to be associated with domesticated animals. For example, serovar canicola (L. canicola) has adapted itself to canines. This has led it to

Wannapong Triampo is with the R&D Group of Biological and Environmental Physics (Biophysics), Department of Physics, Faculty of Science, Mahidol University, Bangkok 10400, Thailand, e-mail:wtriampo@yahoo.com.

Doangkamol Baowan is with the Department of Mathematics, Faculty of Science, Mahidol University, Bangkok 10400, Thailand, I

Ming Tang is with the Department of Mathematics, Faculty of Science, Mahidol University, Bangkok 10400, Thailand, e-mail: imingtang@yahoo.com.

Narin Nuttavut is with the R&D Group of Biological and Environmental Physics (Biophysics), Department of Physics, Faculty of Science, Mahidol University, Bangkok 10400, Thailand, e-mail:narinnuttavut@yahoo.com. Jirasak

Wong-Ekkabut is with the R&D Group of Biological and Environmental Physics (Biophysics), Department of Physics, Faculty of Science, Mahidol University, Bangkok 10400, Thailand, e-mail:jirasakwo@hotmail.com.

Galayanee Doungchawee is with the Department of Pathobiology, Faculty of Science, Mahidol University, Bangkok 10400, Thailand. e-mail:scylb@mahidol.ac.th.

become common in many human communities. Epidemiologic investigation of leptospirosis is often hampered by the difficulty of making a definitive microbiologic diagnosis. Isolation of leptospira from clinical samples provides a definitive diagnosis. However, the value of this technique is limited because prolonged incubation periods are needed before the bacteria's are detectable.

In Thailand, leptospirosis is becoming a major concern of the public health officials and control strategies are being developed. It is a notifiable disease, and reported cases are investigated by the Division of Epidemiology, Ministry of Public Health. The number of leptospirosis cases reported in 1999 was 6,080 (incidence 9.89/100,000/year) [6]. The number reported in 2000 was 14,286 (incidence 23.13/100,000/year) [7] and in 2001, the number was 10,217 (incidence 16.45/100,000/year) [8]. It occurs mainly in the rainy season, with an increase in cases beginning in August, reaching a peak in October, and beginning to fall in November.

In this paper, we model the spread of the leptospirosis using the susceptible-infective-removed (SIR) model that has been used to describe the transmission dynamics of many infectious diseases. Modification of the SIR model must be made it applicable to a particular disease [9].

II. MODEL

The SIR model was initially proposed by Kermack and Mckendrick [10]. Common to most SIR models is division of the players into the human population and the vector population, which in the case of leptosprosis are rats. The human population is then divided into three groups; S_H^* – susceptible human, I_H^* – infected human, and R_H^* – removed human. The vector population is divide into two subgroups, S_A^* – susceptible vector, and I_A^* – infected vector. In many of the SIR models, the following assumptions are made:

- a. The total size N of human population is constant.
- b. The natural death constant rate λ_H is taken to be the same for all population subgroups.
- c. The individuals are unaffected by age or disease status so that the vital statistics of all individuals are the same. Thus the life expectancy is the same for everyone and is $1/\lambda_H$.
- d. Deaths are balanced by births (birth rate being μ_H). This leads to condition 'a.'

- e. All newborn are considered not to be immunized and so become vulnerable instantly.
- f. There is spatially homogeneous mixing among vector and human populations.

In addition to these common assumptions, there are a few assumptions particular to the spread of leptosprosis and a few other diseases:

i.Only infected vectors can be infected human. This means that an infected human can

not infected another human.

ii. Infected humans can not infect the susceptible vectors.

iii.Once infected, a susceptible vector (S_A^*) becomes instantly infectious vector (I_A^*) with no incubation time

instantly infectious vector (I_A) with no incubation time needed for the infectious agents (leptospira) to develop.

iv. The infected human can be cured by the antibiotic medicines and they become immune at a rate (r_1) .

v. Immune individuals become susceptible (S_{H}^{st}) again at a constant rate r_{2} .

vi.The rate of transmission of leptosprosis from an infected vector to a susceptiable human varys with the amount of rain fall according to some Gaussian distribution dependence.

The diagram representing the dynamics of transmission of Leptospirosis is shown in Fig. 1. Based on the common assumptions given by (a.) to (f.) and the special assumptions given by (i.) to (vi.), we have the following equations;

$$\frac{dS_{H}^{*}}{dt} = \mu_{H}N_{H} - \lambda_{H}S_{H}^{*} - \gamma_{H}^{*}I_{A}^{*}S_{H}^{*} + r_{2}R_{H}^{*}$$
(1)

$$\frac{dI_{H}^{*}}{dt} = \gamma_{H}^{*} I_{A}^{*} S_{H}^{*} - \lambda_{H} I_{H}^{*} - r_{1} I_{H}^{*}$$
 (2)

$$\frac{dR_H^*}{dt} = r_1 I_H^* - \lambda_H R_H^* - r_2 R_H^*$$
 (3)

Here $S_H^*(t) + I_H^*(t) + R_H^*(t) \equiv N_H^*(t) = N_H^*(t_0)$ denotes the number of the total population, which is kept constant. The positive constant γ_H is the average number of contacts per infective individual per month.

For the vector populations, we have

$$\frac{dS_{A}^{*}}{dt} = \mu_{A}S_{A}^{*} - \lambda_{A}S_{A}^{*} - \gamma_{A}^{*}S_{A}^{*}I_{A}^{*}$$
 (4)

$$\frac{dI_{A}^{*}}{dt} = \mu_{A}I_{A}^{*} - \lambda_{A}I_{A}^{*} + \gamma_{A}^{*}S_{A}^{*}I_{A}^{*}$$
 (5)

 μ_A and λ_A are the birth and death rate respectively. We have assumed that all newborns have the same status as their parents.

We normalize the variables in (1)-(5), based on the assumption that the number of population is constant, by

letting

$$\begin{split} S_H &= S_H^* \ / \ N_H \ , \ I_H = I_H^* \ / \ N_H \ , \ R_H = R_H^* \ / \ N_H \ , \\ S_A &= S_A^* \ / \ N_A \ , \ I_A = I_A^* \ / \ N_A \ , \ \gamma_H = \gamma_H^* N_A \ , \ \text{and} \\ \gamma_A &= \gamma_A^* N_A \ \ \text{then we obtain} \end{split}$$

$$\frac{dS_H}{dt} = \mu_H - \lambda_H S_H - \gamma_H I_A S_H + r_2 R_H \tag{6}$$

$$\frac{dI_H}{dt} = \gamma_H I_A S_H - \lambda_H I_H - r_1 I_H \tag{7}$$

$$\frac{dR_H}{dt} = r_1 I_H - \lambda_H R_H - r_2 R_H \tag{8}$$

$$\frac{dS_A}{dt} = \mu_A S_A - \lambda_A S_A - \gamma_A S_A I_A \tag{9}$$

$$\frac{dI_A}{dt} = \mu_A I_A - \lambda_A I_A + \gamma_A S_A I_A \tag{10}$$

Because of constraints $S_H + I_H + R_H = 1$ and $S_A + I_A = 1$, the above system of equations can be simplified into the following three equations.

$$\frac{dI_{H}}{dt} = \gamma_{H} I_{A} (1 - I_{H} - R_{H}) - I_{H} (\mu_{H} + r_{1})$$
(11)

$$\frac{dR_H}{dt} = r_1 I_H - R_H (\mu_H + r_2)$$
 (12)

$$\frac{dI_A}{dt} = \gamma_A I_A (1 - I_A) \tag{13}$$

The steady-state solutions are determined by setting

$$dI_H / dt = 0$$
, $dR_H / dt = 0$,

 $dI_A/dt = 0$; the nontrivial solution is

$$\overline{E}_{2}=\left(I_{H}^{\prime}\,,R_{H}^{\prime}\,,I_{A}^{\prime}\right)$$
 , where

$$I'_{H} = \frac{\gamma_{H}}{\gamma_{H} + \frac{\gamma_{H}r'_{1}}{\mu_{H} + r_{2}} + (\mu_{H} + r_{1})}$$

$$R'_{H} = \left[\frac{\gamma_{H}}{\gamma_{H} + \frac{\gamma_{H}r_{1}}{\mu_{H} + r_{2}} + (\mu_{H} + r_{1})} \right] \frac{r_{1}}{\mu_{H} + r_{2}}$$

and

$$I'_A = 1$$

III. NUMERICAL RESULTS AND DISCUSSION

The model described by Eqs. (11)-(13) can be integrated numerically using a fourth-order Runge-Katta method. Time step of 2.2 (corresponding to 6 days in real time) is used. Since we know the numbers of infected human with leptospirosis disease in 2000 and 2001, reported by the Ministry of Public Health of Thailand, we should be able to reproduce data using simulation methods to find the values of some of the parameters appearing in the three equations. We pick the first point to be May in order to match the beginning of the raining season and other points to be one month until we reach the end of April. In term of the infected people, we normalize the number of the patients in every month by the total number of them in each year for representation on the graph. We do the same to the data for the amount of the rain as reported by Department of Meteorology in Fig.2. We fit the graphs using a Gaussian fitting to the 12 data points. The Gaussian fitting equation used is

$$y = y_0 + \frac{A}{w\sqrt{\pi/2}}e^{-\frac{2(x-x_c)^2}{w^2}}$$

In this study, we will see that behavior of the epidemic at the local levels is the same as that at the national level (Thailand as a whole). We have picked Phrae province, located in the north of Thailand, and Nakhon Ratchasima province, located in the north-east of Thailand, to study. These two provinces are isolated from each other and rats are hardly moving from Phrae to Nakhon Ratchasima so they are nothing in common. Moreover, both of them are in the list of the ten provinces having the highest rate of infection (See Fig. 3.).

Using the special condition (vi), we obtain the changes in the transmission rate of the leptosprosis to humans for each month. A one month scaling was used since the Leptospira requires one month to develop. A brute force method was used to determine the initial values of parameters such as the number of infected human, the number or removed human, and the number of infected vectors. The values of certain parameters of the model such as the birth rate, the death rate, and the population size, were obtained from the demographic data of each area. The life expectancy of a human $(1/\lambda_H)$ is about 60 years old and so the mortality rate of the human ($\lambda_{\rm H}$) is $1/(365 \times 60)$ per day. The life span under natural conditions of the vectors (rats) is one and a half year. Therefore, the death rate of the vectors (λ_v) is $1/(1.5 \times 365)$ per day. The recovery rate of an infectious human, or immunity (r_1) , is 1/15 per day. The rate of loss of immunity (r_2) is taken to be 1/360 per day. The transmission rate ($\gamma_{H}\,\mathrm{or}\,\gamma_{A})$ depends on We have only considered the possible dependence on the amount of rain fall. We have assumed that the transmission rate of leptosprosis from an infected vector to a susceptible vector to be a constant.

Fig. 4 shows the temporal evolution of I(t) in 2000 and 2001 in the Phrae province and Nakhon Ratchasima. The star data represents the actural data and the closed circle lines represent the values obtained by solving equations (11)-(13). We then use the data of on the total number of infected people in Thailand during the years of study and the rain fall all over the country in the year, we will obtain the figure shown in Fig. 5

IV. CONCLUSION

In this paper, we have seen that number of cases of

leptosprosis infections in two provinces, Phrae province and Nakhon Ratchasima province, and throughout Thailand obtained by solving a SIR model of the transmission of this diseases in 2000 and 2001 are in good agreement with the actural incidence rates if the transmission rate of leptosprosis from the vectors to the human is taken to be correlated to the rain fall. Why this happens is still a matter of conjecture. In forthcoming works we expect to generalize the model becoming more realistic model including the time delay of the

TABLE I
TOP TEN RATES PER 100000 PERSONS OF LEPTOSPIROSIS DISEASE IN
THAIL AND IN 2000

THAILAND IN 2000		
Provinces	Infected rate per 100000 persons	
1. Buri Ramx	207.90	
2.Nong Bua Lam Phu	138.17	
3.Loei	135.94	
4.Surin	84.72	
5.Khon Kaen	75.80	
6.Phrae	71.07	
7.Nakhon	57.95	
Ratchasima		
8.Chaiyaphum	51.23	
9.Kalasin	44.51	
10.Maha Sarakham	41.75	

From: Annual epidemiological surveillance report 2000, Bureau of epidemiology department of disease control Ministry of Public Health Thailand, Thailand.

TABLE II Top ten rates per 100000 persons of leptospirosis disease in Thailand in 2001

Provinces	Infected rate per 100000 persons
1.Loei	207.90
2.Phrae	138.17
3.Surin	135.94
4.Khon Kaen	84.72
5.Nong Bua Lam Phu	75.80
6.Roi Et	71.07
7.Chaiyaphum	57.95
8.Buri Ram	51.23
9.Nakhon	44.51
Ratchasima	
10.Amnat Charoen	41.75

From: Annual epidemiological surveillance report 2001, Bureau of epidemiology department of disease control Ministry of Public Health disease diffusion that may provide some enlightenment.

V. ACKNOWLEDGEMENT

This research is supported in part by The Thailand Research Fund (TRF), the National Center for Engineering and Biotechnology, Thailand (BIOTEC), the Institute of Innovation and Development of Learning Process(IIDLP), The Third World Academy of Sciences (TWAS), The Royal

Golden Jubilee Ph.D. Program (PHD/0240/2545) to Jirasak Wong-ekkabut, Development and Promotion of Science and Technology talents (DPST) to Duangkamon Baowan are acknowledged.

APPENDIX

Fig. 1 Flowchat of the dynamics of transmission of Leptospirosis.

Fig. 2 Gaussian fitting of the rain from May to April. The rainfall for 2000 is in a) with $Chi^2=0.00102,\ R^2=0.6353,\ y_0=0.04232\pm0.02033,\ x_c=6.77107\pm1.08999,\ w=5.51086\pm2.88476,\ {\rm and}\ A=0.61819\pm0.38179.$ The rainfall for 2001 is in b) with $Chi^2=0.00124,\ R^2=0.63694,\ y_0=0.03538\pm0.02324,\ x_c=7.30693\pm0.81597,\ w=5.30834\pm2.40361,\ {\rm and}\ A=0.67135\pm0.3721.$

Fig. 3 Thailand map showing Phrae and Nakhon Ratchasima provinces, in black color. The simulated data obtained from the model were compared to the real data for these two provinces. From http://www.thailand-yellowpages.com/Thai/info/map.html

Fig. 4 The temporal evolution of infected human where the star indicates the actual data and the circles correspond to the simulated results. a) Phrae province in 2000, b) Phrae province in 2001, c) Nakhon Ratchasima in 2000, and d) Nakhon Ratchasima in 2001. All use the same time steps, 2.2 with $\gamma_A=0.2,\ r_1=1/15,\ r_2=1/360$, and with γ_H taken to be dependent on the rainfall during the month

Fig. 5. The temporal evolution of infected human in a) 2000 and b) 2001 where the stars indicate real data while the circles indicate the simulation result. Here, time step = 2.2, γ_A = 0.2, r_1 = 1/15, r_2 = 1/360, and γ_H varies with the amount of rain fall during the month.

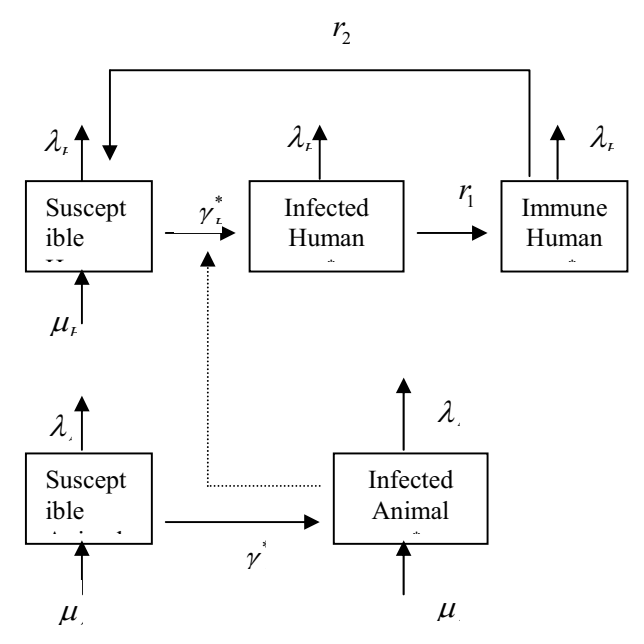


Fig. 1 Flowchat of the dynamics of transmission of Leptospirosis.

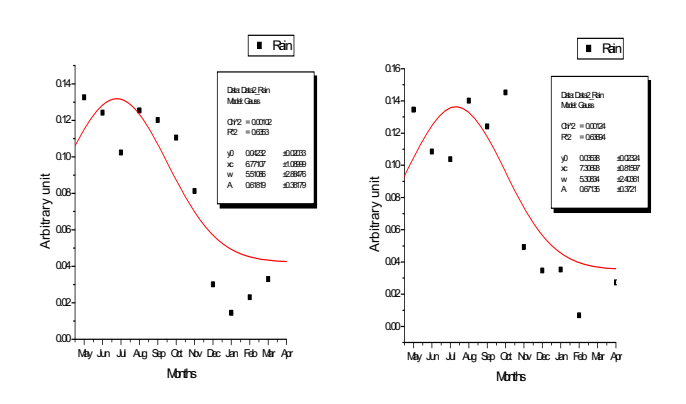


Fig. 2 Gaussian fitting of the rain from May to April. The rainfall for 2000 is in a) with Chi^2 = 0.00102, R^2 = 0.6353, y_0 = 0.04232 \pm 0.02033, x_c = 6.77107 \pm 1.08999, w = 5.51086 \pm 2.88476, and A = 0.61819 \pm 0.38179. The rainfall for 2001 is in b) with Chi^2 = 0.00124, R^2 = 0.63694, y_0 = 0.03538 \pm 0.02324, x_c = 7.30693 \pm 0.81597, w = 5.30834 \pm 2.40361, and A = 0.67135 \pm 0.3721.

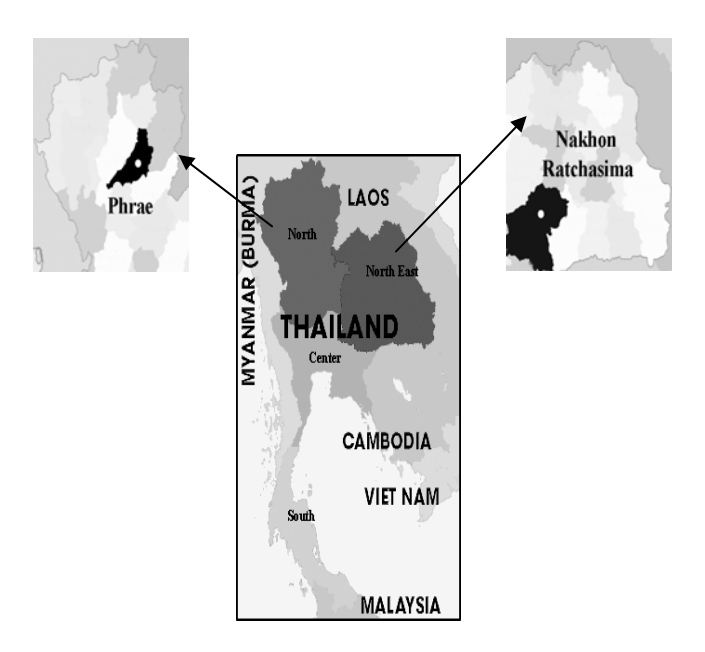


Fig. 3 Thailand map showing Phrae and Nakhon Ratchasima provinces, in black color. The simulated data obtained from the model were compared to the real data for these two provinces. From http://www.thailand-yellowpages.com/Thai/info/map.html

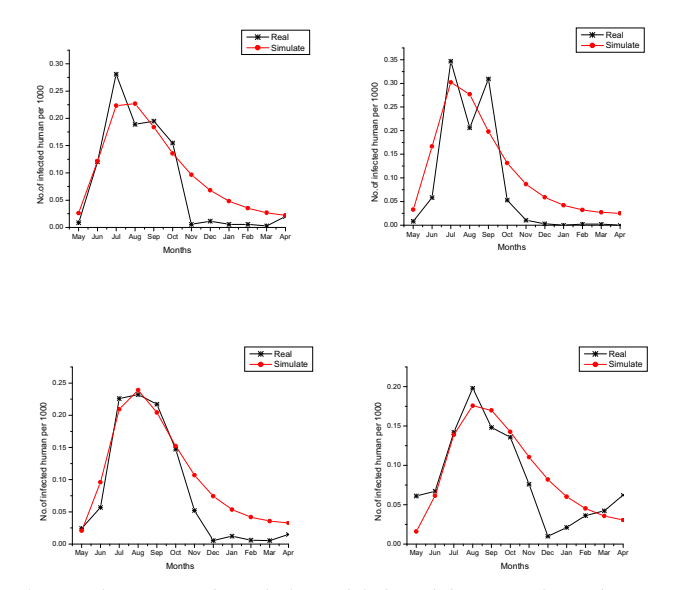


Fig. 4 The temporal evolution of infected human where the star indicates the actual data and the circles correspond to the simulated results. a) Phrae province in 2000, b) Phrae province in 2001, c) Nakhon Ratchasima in 2000, and d) Nakhon Ratchasima in 2001. All use the same time steps, 2.2 with $\gamma_A=0.2$, $r_1=1/15$, $r_2=1/360$, and with γ_H taken to be dependent on the rainfall during the month.

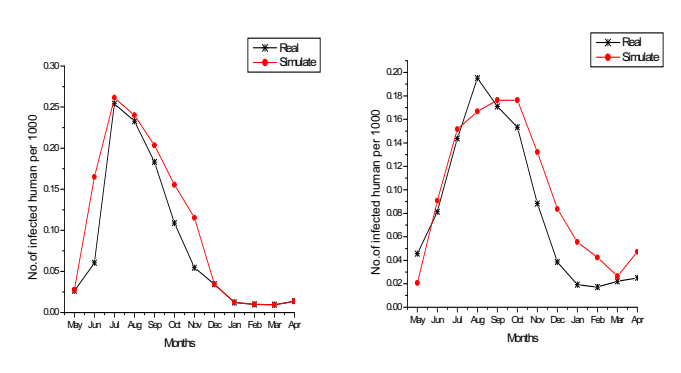


Fig. 5 The temporal evolution of infected human in a) 2000 and b) 2001 where the stars indicate real data while the circles indicate the simulation result. Here, time step = 2.2, γ_A = 0.2, r_1 = 1/15, r_2 = 1/360, and γ_H varies with the amount of rain fall during the month.

REFERENCES

- S. Faine, (ed), Guideline for control of leptospirosis, World Health Organization Geneva, Vol 67, 1982, pp. 129.
- [2] S. Faine, B. Adler, C. Bolin and P. Perolat, Leptospira and Leptospirosis, 2nd ed., MediSci Ed, Melbourne, 1999, pp. 272.
- [3] J.C. Sherris, An introduction to infectious disease, 2nd ed., Elsevier, New York, 1990, pp.432-435.
- [4] L. H. Turner, Leptospirosis I. Trans. R. Soc. Trop. Med. Hyg, Vol 61, 1967, pp.842-855.
- [5] A. S. Benenson and J. E. Chin, (ed.), Control of communicable diseases manual. American Public Health Association, 2000, pp.293-296.
- [6] Reported cases and morbidity rate per 100,000 population of leptospirosis by year in Thailand, (1995-2000), Disease Notification Report, Leptospirosis Control Office 2002.
- [7] Annual epidemiological surveillance report 2000, Bureau of epidemiology department of disease control Ministry of Public Health Thailand, Thailand, 2000, pp.183-189.
- [8] Annual epidemiological surveillance report 2001, Bureau of epidemiology department of disease control Ministry of Public Health Thailand, Thailand, 2001, pp.179-185.
- [9] R. M. Anderson and R.M. May, Infectious Diseases of Humans: Dynamics and Control. Oxford University Press, Oxford, 1991.
- [10] W.O. Kermack and A.G. McKendrick, A contribution to the mathematical theory of epidemics, Proceeding of the Royal Society of London, Vol 115, 1927, pp.700-721.

The Effects of TiO₂ Nanoparticles on Tumor Cell Colonies: Fractal Dimension and Morphological Properties

T. Sungkaworn, W. Triampo, P. Nalakarn, D. Triampo, I. M. Tang, Y. Lenbury, and P. Picha

Abstract—Semiconductor nanomaterials like TiO₂ nanoparticles (TiO₂-NPs) approximately less than 100 nm in diameter have become a new generation of advanced materials due to their novel and interesting optical, dielectric, and photo-catalytic properties. With the increasing use of NPs in commerce, to date few studies have investigated the toxicological and environmental effects of NPs. Motivated by the importance of TiO2-NPs that may contribute to the cancer research field especially from the treatment prospective together with the fractal analysis technique, we have investigated the effect of TiO2-NPs on colony morphology in the dark condition using fractal dimension as a key morphological characterization parameter. The aim of this work is mainly to investigate the cytotoxic effects of TiO2-NPs in the dark on the growth of human cervical carcinoma (HeLa) cell colonies from morphological aspect. The in vitro studies were carried out together with the image processing technique and fractal analysis. It was found that, these colonies were abnormal in shape and size. Moreover, the size of the control colonies appeared to be larger than those of the treated group. The mean Df +/- SEM of the colonies in untreated cultures was 1.085 ± 0.019 , N= 25, while that of the cultures treated with TiO₂-NPs was 1.287±0.045. It was found that the circularity of the control group (0.401±0.071) is higher than that of the treated group (0.103±0.042). The same tendency was found in the diameter parameters which are 1161.30±219.56 μm and 852.28±206.50 μm for the control and treated group respectively. Possible explanation of the results was discussed, though more works need to be done in terms of the for mechanism aspects. Finally, our results indicate that fractal dimension can serve as a useful feature, by itself or in conjunction with other shape features, in the classification of cancer colonies.

Titiwat Sungkaworn is with the Department of Biology and 6R&D Group of Biological and Environmental physics (BIOPHYSICS), Faculty of Science, Mahidol University, Bangkok 10400, Thailand.

Wannapong Triampo is with the Department of Physics and R&D Group of Biological and Environmental Physics (BIOPHYSICS), Department of Physics, Faculty of Science, and Center for Vectors and Vector-Borne Diseases, Mahidol University, Bangkok 10400, Thailand (e-mail:wtriampo@yahoo.com).

Pornkamol Nalakarn is with the 5Department of Physics, Faculty of Science & Technology, Thammasat University, and R&D Group of Biological and Environmental Physics (BIOPHYSICS), Faculty of Science, Mahidol University, Bangkok 10400, Thailand.

Daraporn Triampo is with the Department of Chemistry and R&D Group of Biological and Environmental Physics (BIOPHYSICS), Faculty of Science, Mahidol University, Bangkok 10400, Thailand.

I. Ming Tang is with the Department of Physics, Faculty of Science, Mahidol University, Bangkok 10400, Thailand.

Yongwimon Lenbury is with the Department of Mathematics, Faculty of Science, Mahidol University, Bangkok 10400, Thailand.

Pontipa Picha is with the National Cancer Institute of Thailand, Bangkok 10400, Thailand.

PACS numbers: 85.15.Aa, 87.17. Aa

Keywords—Tumor growth, Cell colonies, TiO₂, Nanoparticles, Fractal, Morphology, Aggregation.

I. Introduction

C EMICONDUCTOR, nanomaterials like TiO_2 nanoparticles (TiO₂-NPs), approximately less than 100 nm in diameter, have become a new generation of advanced materials due to their novel and interesting optical, dielectric, and photo-catalytic properties from size quantization [1]. Therefore, many efforts have been devoted to produce TiO₂-NPs with controlled size, shape, and porosity for use in thin films, ceramics, composites, and catalysts. These nanometersized effects are caused by the large surface-to-volume ratio, resulting in more atoms along the grained boundaries than in the bulk material. It is known that the more the particles decrease in size the more attractive interactions between the particles become dominant. These attractive forces lead them to aggregate or agglomerate when the particles collide resulting in nanoparticle aggregates (NPAs) (see Fig. 1). Since the desired product properties might vary with particle size as well as the degree of aggregation or the aggregate structure, control of the particle size distribution and the aggregate structure is a key criterion to product quality. It has been accepted that NPs can exist in two states within a liquid: stable, i.e. particles separate, non-adhering and dispersed, and aggregated or flocculated, i.e. adherent and randomly clumped [2]. This clumping can occur due to van der Waals attractive forces or may be caused by magnetic or other attractions imposed by externally imposed fields. To calculate the particle-particle interaction, the DLVO theory can be employed [3]. Hence, it is very important to realize that the NPs being used in experiments, especially in suspension or colloid form have the properties (e.g., size distribution) which are different from those specified by manufactures. Moreover, in experimental processes such as sonicator, autoclave, pH and so on, may change the state or properties of the particles. Therefore, using NPs in experiments must be done with care.

With the increasing use of NPs in commerce, to date few studies have investigated the toxicological and environmental effects of NPs. Exposure to nanoparticle substances can be an important risk factor for human health. The sub-micron size of NPs offers a number of distinct advantages over

microparticles (MPs). NPs have in general relatively higher tracellular uptake rate compared to MPs. This was demonstrated in studies in which 100 nm size NPs showed 2.5 fold greater uptake compared to 1 mm and 6 fold higher uptake compared to 10 mm NPs in Caco-2 cell line [4]. Similar results were obtained when these formulations of NPs and MPs were tested in a rat in situ intestinal loop model. The efficiency of uptake of 100 nm sized particles was 15–250 fold greater than larger sized (1 and 10 mm) MPs [5]. In the above rat study, it was found that NPs were able to penetrate throughout the submucosal layers while the larger size MPs were predominantly localized in the epithelial lining.

TiO2 or titania could be used as an alternative or a complement to conventional biocidal activity technologies via photocatalysis. Photocatalytic events that occur after UVA/UVB with wavelength of less than 385nm (365< wavelength < 385) illumination of TiO₂ (band-gap energy of anatase, 3.2 eV; for rutile, 3.0 eV) and subsequent formation of electron/hole pairs are many and very complex. Following electron/hole separation, the two charge carriers migrate to the surface through diffusion and drift, in competition with a multitude of trapping and recombination events in the lattice bulk. At the surface, these carriers are poised to initiate redox chemistry with suitable pre-adsorbed acceptor and donor molecules in competition with recombination events to yield radiative and nonradiative emissions, and/or trapping of the charge carriers into shallow traps at lattice sites (e.g., anion vacancies, Ti4+, and others). Thus, on absorption of UV light, titania particles yield superoxide radical anions and hydroxyl radicals that can initiate oxidations [6]. Photocatalytic biological inactivation has been explained by the attack of Oxygen-derived molecular species or reactive oxygen species (ROS), especially radicals photogenerated at the surface of the TiO_2 catalyst like O_2^- , HO_2 and OH. mechanism of cell death or damage has not been understood yet [7].

Oxygen-derived molecular species or reactive oxygen species (ROS), such as superoxide (O_2^-) and hydrogen peroxide (H_2O_2) , are produced in cells as a result of aerobic metabolism. Excess generation of these species can result in damage to macromolecules such as DNA and lipids [7].

Many studies using TiO₂ photodecomposition of pollutants with the aim of developing methods to purify water and air have been carried out [8],[9],[10],[11]. For the bactericidal activity, several results have been reported using TiO₂ powder [12],[13],[14],[15],[16], and, TiO₂-coated materials for this purpose [17]. However, few studies have investigated the impacts of TiO₂ in cancer science or the field of oncology [18]. However, the actual factors that control the photocatalytic activity of specific TiO₂ particles are still unknown. Moreover, the detailed studies of the effects of TiO₂ on biological systems in dark condition were very rare. This is one of the reasons that motivate us to perform this study.

Cancer has been a leading cause of human death in the world. Not too much is known about the biological mechanisms leading to the establishment of or the growth of

malignant tumors. Many attempts have been made in recent decades to describe the basic biological mechanisms of tumor growth. Benign masses generally have smooth, circumscribed, and well-defined contours, whereas malignant tumors commonly have rough, spiculated, and ill-defined contours. Based upon this observation, shape or morphological factors such as fractal dimension (Df) have been considered.

Fractal patterns arise "spontaneously" in natural processes as a result of many microscopic interactions, and the fractal dimension is a precise measure of the morphology of a complex pattern [19],[20]. Fractal geometry is a way of quantifying natural objects with a complex geometrical structure that are difficult to quantify by regular Euclidean geometrical methods. In classical Euclidean geometry, objects have integer dimensions. For example, a line is a onedimensional object, a plane a two-dimensional object, and a volume a three-dimensional object, with dimensions of 1, 2 & 3 respectively. In this way, Euclidean geometry is suited for quantifying objects that are ideal, man-made, or regular. One of the most important features of fractal objects is that they are self-similar; i.e., there is a repetition of patterns in the object at many different scales. In nature there is a wide range of self-organized spatial structures in multiple hierarchical levels. Surface morphology or roughness can be quantified by the value of fractal dimension, a numerical parameter having emerged from the fractal theory. This theory provides a new way to characterize irregular structure. Fractal dimension (Df) measures the space filling capacity of an object. In a fractal system, the fractal dimension of the system is less than the dimension d of the space in which the system is embedded. In recent years, the geometry of fractals has been applied to a surprising set of phenomena including electrochemical deposition [21], the architecture of physiological systems such as the bronchial tree [22], taxonomy [23], and clusters of stars [20]. Study of the fractal structure has intensified in a number of biological structures and their growth patterns in past recent years[24],[25],[26],[27],[28],[29],[30],[31],[32],[33],[34],[35]

Motivated by the importance of TiO₂-NPs that may contribute to the cancer research field especially from the treatment prospective combined with the fractal analysis technique that has proved to be useful in many fields including life science, the aim of the present study was to investigate the effect of NPs on colony morphology using fractal dimension as a key morphological characterization parameter. To the best of our knowledge, this is the first published literature on this problem.

II. MATERIALS AND METHODS

A. TiO₂ Nanoparticles

 ${
m TiO_2}$ (P25, Sigma-Aldrich) with a surface area of 10-20 m²/g and primary particles whose size of 60-100 nm were used in experiments. The particles were suspended in sterile water and sonicated for 15 min before experiment. All processes were performed in darkness.

B. Cell Culture

Human cervical carcinoma cells (HeLa), obtained from National Cancer Institute, Thailand were cultured in EMEM (BioWhittaker), pH 7.2, supplemented with 10% NCS (BioWhittaker), penicillin (100 U/ml) and streptomycin (100 μ g/ml) at 37°C in a humidified atmosphere of 5% CO₂.

C. Colony-Forming Assay

HeLa cells in exponential phase were trysinised and counted by a Hemocytometer. Then, cell suspension was diluted and plated in 6 well cultured clusters (Corning) with TiO₂. Sterile water was used as control. After culturing for 10 days, the colonies were stained with 10% Giemsa solution (Merk) and then photographed under inverted microscope with a coupled digital camera. If the cell colony is successfully grow, i.e., colony forming efficiency more than 80% control condition, (the size and shape of the cells are as shown in Fig. 2.), the morphology will be observed by inverted phase-contrast microscopy and analyzed.

D. Image Processing and Fractal Dimension Calculation

Image processing and fractal dimension (Df) calculation via the box-counting method (BCM) were performed by using ImageJ shareware program from NIH Laboratory (http://rsb.info.nih.gov/ij/). BCM, is one of the most widely used [36],[37],[38] due to the relative ease of mathematical calculations and computations involved. It basically consists of drawing successively larger boxes and counting the number of boxes that touch particles (any color different from background color). The slope of the log-log plot of the number of boxes vs. their respective size is the fractal dimension.

For image processing (see Fig. 3), firstly, the acquired images were converted from RGB to 8-bit format images. Via automatic default threshold function, we can get black and white images with binary bit, namely 0 (totally black) to 255 (completely white). We then "clean up" the image and leaving only the boundary outline with the image of size 2592 x 1944 (this is one of the control parameters). Finally, we can evaluate the fractal dimension with the output sample as seen in Fig. 4.

To have confidence in our tool as to whether the software is installed or set up properly, the BCM has then been validated with a known fractal dimension structure. For the triangular Sierpinski gasket 12, the initiator is a filled triangle shown as Fig. 5. The fractal curve obtained in the limit of an infinite number of generations has the fractal dimension $D = \ln 3/\ln 2 = 1.585$. The dimension obtained by the box size method using ImageJ software is equal to 1.579, which is accurate up to 0.379%. In addition, we also tested the software on the Koch Curve 6, and it was found that, with the theoretical value = 1.262, a our software yielded 1.267, so that the error is within 1.041% (see Fig. 5).

III. RESULTS AND DISCUSSION

In this section we present some experimental results of TiO_2 -NPs-induced changes in cell colonies. Tumor cell colonies were grown in vitro, so that the nutrient concentration was uniform along the colonies. A control set of colonies was grown without TiO_2 -NPs and a treatment set of colonies was cultured at a concentrations or dose of TiO_2 -NPs = 400 ppm. In this study, we have applied a fractal index as key parameter to characterize the colony morphology that features the growth.

Growth and development of living organism populations shows a great variety of geometrical shapes. The aim of the present study was to investigate the effect of TiO₂-NPs on the colony morphology of tumor cell colony in vitro. Our results demonstrate that it is possible to describe how a cell colony adapts itself to external changes, from morphological points of view. However, the way in which an ensemble of cells forms a colony, usually via cell motility and cell–cell adhesion, is not fully understood at the sub-cellular level. More experimental and theoretical works especially with regards to the mechanism aspect are needed.

Fig. 6 shows typical colonies at different culture conditions, namely with control and treatment conditions. It was clearly observed that colony growth is morphologically changed from control when treated with TiO₂-NPs. It was also found that, these colonies were abnormal in shape and size. In addition, the size of the control colonies appeared to be larger than those of treated group as seen in Fig. 7. The mean diamerter +/- SEM of the colonies in untreated cultures was $1,161.302\pm219.566\mu m$, N= 25, while that of the cultures treated with TiO2-NPs was 852.284±206.497 µm (see table 1). Due to the aggregation TiO₂-NPs, the resulting larger sized particles were observable through naked eyes in black dots or patches. This data may evidently indicate the spread and the adsorption of particles which could affect the growth of colonies. However, it should be noted that only the larger sized particles were observed either through naked eyes or OM. The nanosize-particles could be observed by a more powerful microscope such as Scanning Electron Microscope (SEM), Transmition Electron Microsope (TEM), or Atomic Force Microscope (AFM), etc.

In Fig. 8, it was found that the box-counting fractal dimension, Df, of individual colonies was increased substantially over that in control cultures. The mean Df +/-SEM of the colonies in untreated cultures was 1.0852 ± 0.0197 , N= 25 and in cultures treated with TiO_2 -NPs 1.2870 ± 0.0454 (see Table I). The standard deviation, it reflected that the morphologies of abnormal or treated colonies are more rough and fluctuated compared to those of the control samples, which appeared to be more uniform and consistent in shape. It should be noted that all the data in this study show fractal dimensions whose complexity is between a straight line (Df = 1) and a circle (Df = 2).

In Fig. 9, to correlate the morphological changes in fractal dimensions with other well known geometrical parameters, we

calculated the circularity and diameter length using the same software, imageJ. It was found that the circularity of the control group (0.4015±0.07100) is higher than that of the treated group (0.103±0.0421). The same tendency was found in the diameter parameter which is 1161.302±219.5663 µm and 852.284±206.4976 µm for the control and treated groups, respectively. In other words, the degree of roughness of colony boundary of the treated samples is significantly larger than that of the control group as clearly seen from fractal dimension and circularity parameters. The irregular boundaries of tumors can be examined by fractal geometric analysis. Indeed, the box counting method reveals that morphological patterns of the higher order, such as gland-like structures or populations of differentiating cancer cells, possess fractal dimension and self-similarity. Since fractal space is not filled out randomly, a variety of morphological patterns or a functional state arises.

On comparing our results with other studies of the TiO2 that effects cancer cells, Cai R and coworkers [39] investigated the anti-tumor activity of photoexcited TiO2 particles on HeLa cells in vitro. They found that cell cultures were completely killed in the presence of TiO₂ (50 micrograms/ml) with 10-min UV irradiation by a 500-W-Hg lamp. In contrast, very little cell death was observed from TiO2 treatment without UV irradiation. They also suggested that the cells were killed by the OH-. and H₂O₂ produced from photoexcited TiO₂ particles. Kubota Y and co-workers [40] studied photokilling of TiO2 on -24 human bladder cancer. Here, a distinct cell killing effect was observed on cultured T-24 human bladder cancer cells treated with TiO2 plus UV light. They also discussed the possible application of photoexcited TiO₂ particles to cancer treatment as a new anti-cancer modality. Ai-Ping Zhang and Yan-Ping Sun [5] investigated the photocatalytic killing effect of photoexcited TiO2 nanoparticles on human colon carcinoma cell line (Ls-174-t) and studied the mechanism underlying the action of photoexcited TiO2-NPs on malignant cells. When the concentration of TiO2 was below 200 mg/mL, the photocatalytic killing effect on human colon carcinoma cells was almost the same as that of UVA irradiation alone. When the concentration of TiO₂ was above 200 mg/mL, the remarkable killing effect of photoexcited TiO2-NPs could be found. On comparing previous findings with our results, in which samples were treated with TiO₂-NPs alone in the dark, our findings seem to reveal surprisingly new findings. To our knowledge, these results are the first that show the significant toxicity effects of TiO₂-NPs on biological systems under dark condition. This may be partly because of the particle size and/or the chosen measurement index.

To relate our fractal results with the previous ones, we refer to the concept and measurement of fractal dimension by the box-counting method given by [36],[37],[38]. Malignant melanomas in vivo have been investigated and it has been found that the fractal dimension of the boundary of the tumor lies mainly in the range 1.05-1.30 [36],[37] while published experimental data for in vitro and in vivo study of the

boundary of human and animal solid tumors giving with Df in the range 1.09-1.34. Our mean fractal dimension of normal tumor colonies lies in the range 1.0454-1.1129, which agrees well with previous reports, while that of the abnormal colonies lies in the range 1.1848-1.3875 which is relatively high. This evidence may benefit, for example, the clinical trials to be used as an alternative indicator for treatment response of cancers. From biophysics view point, one of the possible explanations of the irregular shape of a colony may be as follows. Due the difference in wave propagation velocities of tumor cell wave (especially at the boundary which are mostly proliferating cells), fluctuations in the number of cell at the front or rim would cause irregularities of its shape and produce irregular cell clusters. Thus, the variety of structural metamorphoses in tumor population waves can be explained both by general approach to their description and by considering individual behavior of cell, with only local interactions between them. These phenomena may be dependent on the essential role of density fluctuations and cell motility in the development of fractal structures. In this particular case where the tumor cells are under the applied stress by being exposed to the TiO2-NPs, the changes in colony morphology may be due to the effect of TiO₂-NPs. that decelerates the proliferation of tumor cells by changing the cell properties. This results in cell death which leads to the loss of adhesion of cells to their substrate leading to the colony change. Another possible explanation may be that the colony should grow until it reaches optimal size; then, all further net energy intake should be allocated to reproduction. This means that the optimal colony size is substantially smaller than the maximum possible colony size when all incoming energy is allocated to maintenance and none is available for reproduction.

IV. CONCLUDING REMARKS

In conclusion, using fractal dimension as a key index for morphological characterization, this paper shows that TiO₂-NPs modify the dynamics of cell colony growth, causing its eventual arrest and resulting in the colony pattern deformation. These findings are somewhat unexpected because the TiO₂-NPs treatment was performed in the dark. Hence, no photocatalytic impact via ROS accounts for the changes. This may emphasize the importance of NPs over MPs. Though the use of fractal index does not normally reveal much about the biological mechanism involved, we believe that fractal analysis here shows its promise as an objective measure of seemingly random structures and as a tool for examining the mechanistic origins of pathological forms. Our results indicate that fractal dimension can serve as a useful feature, by itself or in conjunction with other shape features, in the classification of cancer colonies. It should be noted that a general classification of cell colonies or tumors regarding their fractal dimensions could be misleading. However, study of the fractal structure has intensified on a number of biological structures and their growth patterns in past recent

years. Emerging data show that variation in the fractal dimensions may serve as an indicator or predictive factor in normal versus disease conditions, serving as an objective means to guide the clinicians.

V. ACKNOWLEDGEMENT

We would like to thank our colleagues in Biophysics group at Mahidol University for technical assistance and helpful discussion. This research work was financially supported in part by The Thailand Research Fund (TRF), the National Center for Engineering and Biotechnology, Thailand (BIOTEC), the Institute of Innovation and Development of Learning Process (IIDLP), The Third World Academy of Sciences (TWAS) and Institute of Science and Technology for Research and Development, Mahidol University.

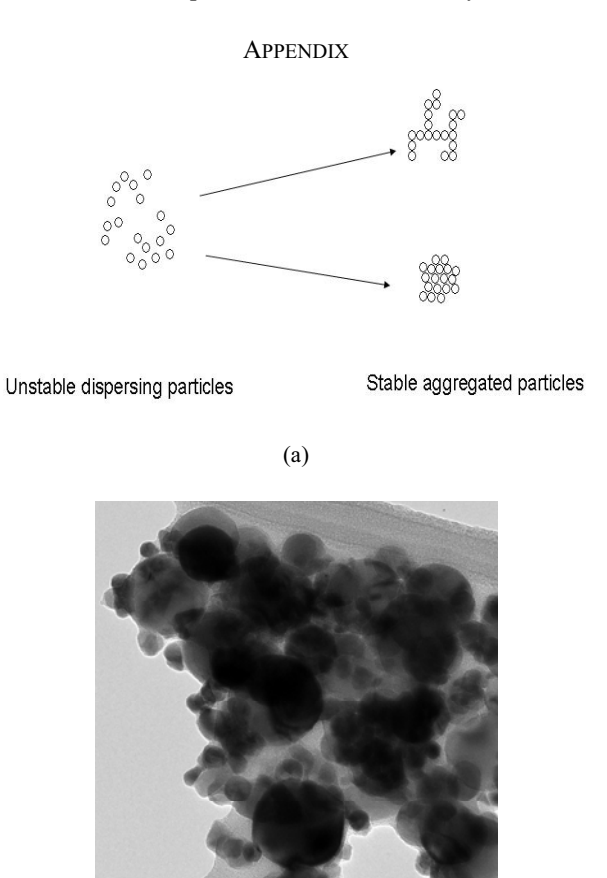


Fig. 1 (a) Schematic picture of unstable dispersing TiO_2 nanoparticles (left) and more stable TiO_2 aggregated particles (right). (b) TEM micrograph of the TiO_2 nanoparticles used in our experiments. The samples were examined under a transmission electron microscope (TECNAI 20) with magnification x29,000

(b)

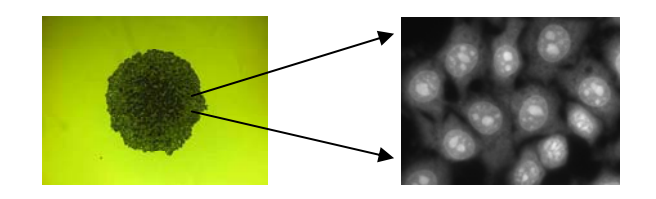


Fig. 2 Example of HeLa cell colony under normal condition (left) and typical individual cells (right). The samples were prepared using the techniques as described in text

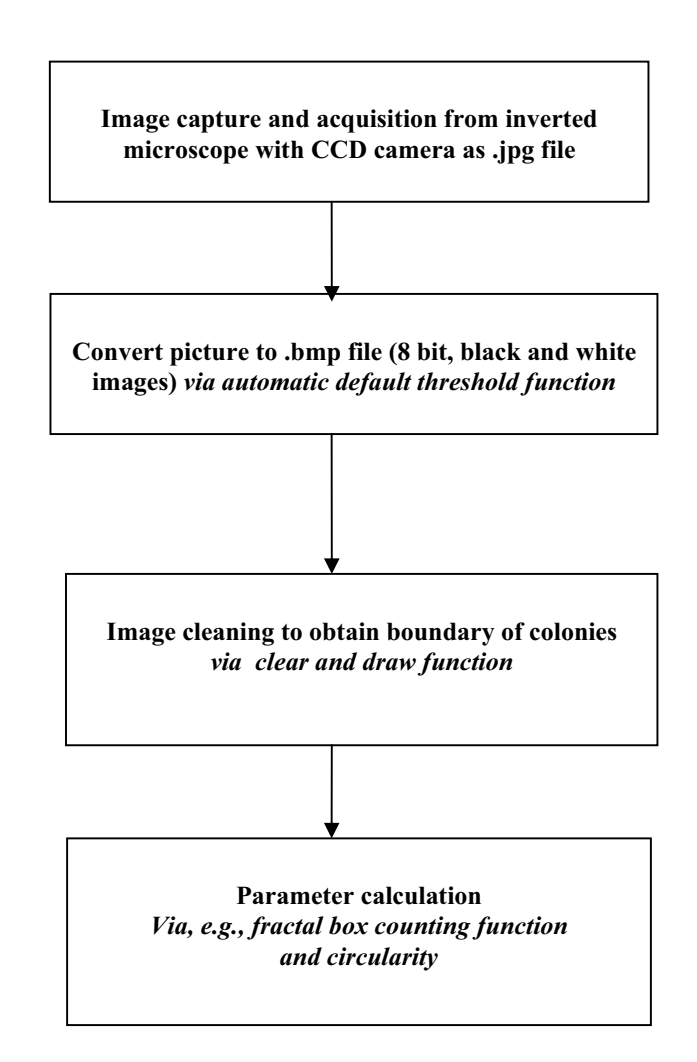
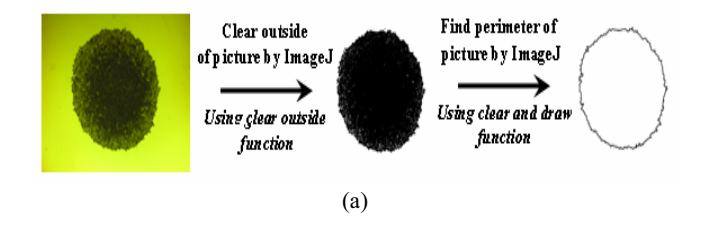


Fig. 3 Flowchart of procedures of image acquisition and parameter calculations



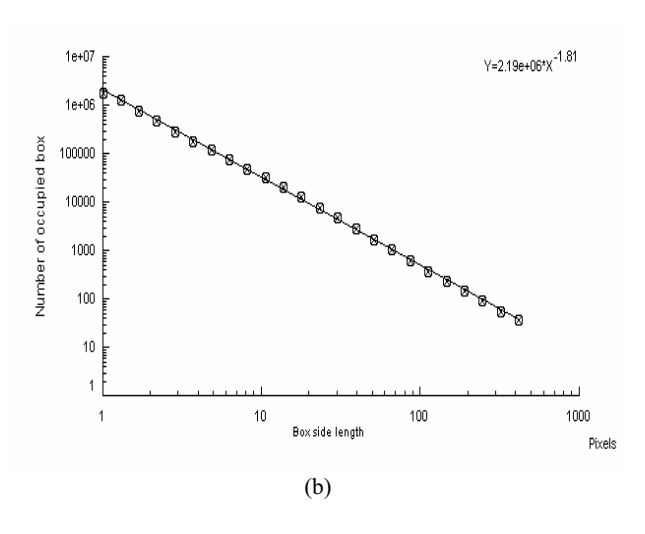
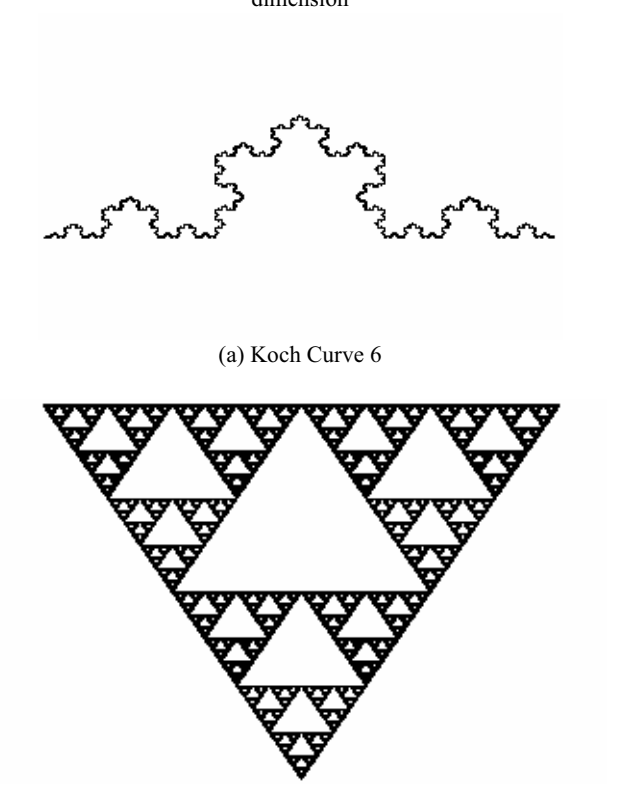


Fig. 4 The fractal dimension interface from imageJ: (a) Diagram of image processing sequence, (b) showing the regression Log-Log plot of boxside-length vs. occupied box number for estimation of fractal dimension

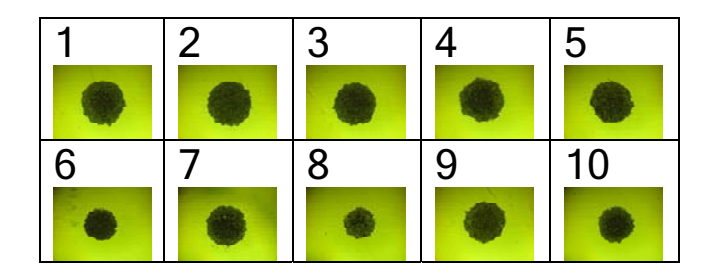


(b) Sierpinski Gasket 12

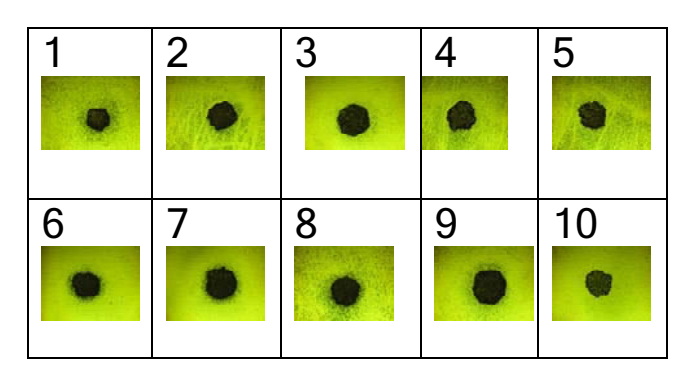
Fig. 5 Tested fractal objects for reliability of the fractal estimation software using in comparison with known theoretical results. Using (a) Koch Curve 6 and (b) Sierpinski Gasket 12. The tests were performed using ImageJ. The test results give: Koch Curve 6 theory =1.262, ImageJ =1.2229, error = 3.098 %, Sierpinski Gasket 12, theory=1.585, ImageJ=1.6015, error = 1.041%.

TABLE I
MEAN VALUES (+/- SEM) OF CELL COLONIES

Parameters	CONTROL GROUP	Treated group
Cell colony Fractal dimension	1.0852±0.019	1.287±0.045
Cell colony circularity	0.4015 ± 0.071	0.103 ± 0.042
Cell colony diameter(µm)	1,161.30±219.56	852.28±206.50



(a) Control or untreated colonies



(b) Colonies treated with 400 ppm. of NPs

Fig. 6 Experimental data of typical colonies: (a) control or untreated colonies and (b) colonies treated with 400 ppm. of TiO₂- NPs